



## ORIGINAL ARTICLE

# Inhibition of stemness and EMT by taxifolin ruthenium-p-cymene complex via downregulating the SOX2 and OCT4 expression on lung cancer



Abhijit Das<sup>a</sup>, Balaram Ghosh<sup>b</sup>, Sandipan Dasgupta<sup>c</sup>, Ishita Seal<sup>a</sup>, Sidhanta Sil<sup>a</sup>, Souvik Roy<sup>a,\*</sup>

<sup>a</sup> Department of Pharmacy, NSHM Knowledge Campus- Kolkata, 124 B.L. Saha Road, Kolkata 700053, West Bengal, India

<sup>b</sup> Department of Pharmacology, Midnapur Medical College, Midnapur, Paschim Midnapore, West Bengal, India

<sup>c</sup> Department of Pharmaceutical Technology, Maulana Abul Kalam Azad University of Technology, Simhat Haringhata, Nadia 741249, West Bengal, India

Received 14 December 2022; accepted 10 May 2023

Available online 16 May 2023

## KEYWORDS

Taxifolin;  
Ruthenium-p-cymene;  
Stemness;  
Epithelial-to-mesenchymal transition;  
Lung cancer

**Abstract** Lung carcinoma is perhaps the most often reported cancer incidence throughout the world. The flavonoid metal complexes have exhibited a potential chemotherapeutic effect. This study investigated the chemotherapeutic effect of taxifolin ruthenium-p-cymene complex against lung carcinoma through MTT assay, transwell migration assay, sphere formation assay, western blot, histopathology, immunohistochemistry, and TUNEL assay. The *in silico* study determined the target proteins of the complex. The synthesized organometallic complex was characterized via various spectroscopical techniques. The complex exhibited strong binding affinity for PI3K, EGFR, and  $\beta$ -catenin. The complex promoted apoptosis and inhibited the colony formation of the cancer cells. Moreover, the cancer cell migration and cancer stemness were reduced with decreased SOX2 and OCT4 expression. The complex induced cell cycle arrest at sub G0/G1 phase, S phase and G2/M phase and promoted caspase-3 mediated apoptosis. The *in vivo* study demonstrated successful restoration of lung tissue due to the treatment with the complex in benzo- $\alpha$ -pyrene induced lung cancer model. Additionally, the expression of p53 and caspase-3 was increased with significant downregulation of Akt, mTOR and  $\beta$ -catenin. In conclusion, the complex inhibited cancer cell viability, stemness, and EMT in both *in vitro* and *in vivo* model systems through the alter-

\* Corresponding author at: Department of Pharmacy, NSHM knowledge campus –Kolkata, 124 B.L. Saha Road, Kolkata 700053, India. E-mail addresses: [dasabhijit070@gmail.com](mailto:dasabhijit070@gmail.com) (A. Das), [sandipan.dasgupta21@gmail.com](mailto:sandipan.dasgupta21@gmail.com) (S. Dasgupta), [souvik.roy@nshm.com](mailto:souvik.roy@nshm.com) (S. Roy).

Peer review under responsibility of King Saud University.



ation of PI3K/Akt/mTOR/EGFR pathway and expression of stem cell markers including SOX2 and OCT4 that eventually abrogated the EMT mediated metastasis of cancer cells.

© 2023 Published by Elsevier B.V. on behalf of King Saud University. This is an open access article under the CC BY-NC-ND license (<http://creativecommons.org/licenses/by-nc-nd/4.0/>).

## 1. Introduction

Lung cancer (LC) is indeed the world's deadliest and most expensive cancer, associated with 2,206,771 new cases and 1,796,144 fatalities. These reports suggesting that the lung cancer has the highest prevalence and mortality levels in the world (Sung et al., 2021). In India, it is also a big healthcare issue. It is estimated that, the incidence of lung cancer will rise to 111,428 cases in 2025 in India (Nath et al., 2022).

Cancer stem cells (CSCs) can be identified as a type of stem cells which are associated with the development of tumor, drug resistance, cancer relapse and epithelial-to-mesenchymal transition (EMT) mediated cancer cell metastasis. The cancer stemness is regulated by several signaling pathways such as JAK/STAT, Notch, PI3K (Phosphoinositide 3 kinase)/Akt/mTOR, SHH, and Wnt/ $\beta$ -catenin signaling cascade (Masciale et al., 2019). The PI3K/Akt pathway is a cell survival pathway, which is directly correlated with the stem cell progression and its survival. It was also reported that upregulation of PI3K/Akt/mTOR pathway inhibits the process of apoptotic events (Yao and Cooper, 1995). In addition, the faulty Wnt/ $\beta$ -catenin signaling pathway triggers cancer stem cell renewal, proliferation, and differentiation which play a key role in tumorigenesis and therapy response (Zhang and Wang, 2020). Wnt/ $\beta$ -catenin signaling pathway also plays important roles from cancer initiation to metastasis and recurrence, by triggering the EMT (Clevers, 2006). EMT has been also shown to turn cancer cells into stem cells (Mani et al., 2008). Moreover, aberrant accumulation of  $\beta$ -catenin caused mutational inactivation of p53 (Sadot et al., 2001) which disrupts the apoptosis of cancer cells. The loss of apoptotic control promotes cancer cell survival and provides enough time for accumulation of mutations which increase the cancer invasiveness and angiogenesis (Hassan et al., 2014). In order to eliminate cancer relapse, metastasis, and associated disorders, targeted therapy against cancer stem cells is therefore needed which facilitates in-depth research into the effects of targeting CSCs.

The natural bioactive compounds play an important role in the treatment of cancer as it possesses a number of biological activities especially the flavonoids (Heim et al., 2002). Flavonoids exhibit a strong antioxidant activity and neutralize the effects of free radicals due to the presence of hydroxyl groups, and they chelate metal ions (Kumar and Pandey, 2013). Quercetin, an important flavonoid, possesses a wide range of documented anticancer potential (Iacopetta et al., 2017). There are various derivatives of quercetin which are also associated with effective anticancer activity, among which taxifolin (3,5,7,3',4'-pentahydroxyflavanone or dihydroquercetin), an operative flavonoid, abundantly found in olive oil, grapes, in citrus fruits and onions (Min et al., 2019) has been used for our study as a natural bioactive compound. Taxifolin is associated with number of biological and pharmacological activities including antioxidant, anti-inflammatory, hepatoprotective, antiangiogenic properties (Butler, 2006), anti-diabetic, cardioprotective, neuroprotective, anti-alzheimer's disease (Min et al., 2019). The anticancer activity of taxifolin has also been exhibited in several cancer model systems (Butler, 2006). Taxifolin has been actively or passively suggested to suppress stemness and EMT in many tumors. It also facilitates the differentiation of human umbilical cord-derived mesenchymal stem cells to osteoblasts (Córdoba et al., 2015). Furthermore, taxifolin decreases invasive cells, through the inhibition of the EMT (Wang et al., 2020). In the current age, the natural compounds have been functionalized with

the metals developing organometallic complex with significant chemotherapeutic potency towards chemotherapy in order to improve the efficacy of the treatment.

Metal complexes have played an essential part in therapy due to their wide range of physico-chemical characteristics which include variable oxidation states, hydrophobicity and lipophilicity, aqueous solubility and positively charged nature (Raj et al., 2018). In this regard, the ruthenium complexes exhibited impressive outcomes as new potential chemotherapeutic agent because of their higher rate of ligand exchange, variable oxidation states, and excellent aqueous solubility and stability in a biological environment (Allardyce and Dyson, 2001). Subsequently, for the better cellular accumulation and better cellular uptake a  $n^6$ -p-cymene moiety has been attached to the ruthenium (Bugarcic et al., 2009). The hydrophobic nature of the ruthenium-attached arene ligand promotes the passive diffusion of the complex through the membrane of the cell and increases the deposition within cells (Dyson, 2017). Once they have planar aromatic ligands, ruthenium(II) complexes may undergo intercalation and the complex is incorporated in between neighboring DNA base pairs (Huang et al., 2014).

In this research, we have synthesized a ruthenium based organometallic complex by using taxifolin and ruthenium-p-cymene and evaluated the anticancer potential of the complex against lung cancer by inhibiting the stemness and EMT. The chemotherapeutic study was performed on benzo[*a*]pyrene induced lung cancer model of mice. Along with that, the potential impacts of taxifolin ruthenium-p-cymene complex in two NSCLC cell lines; A549 and NCI-H460 were also assessed in vitro, focusing precisely on its potential to inhibit the cancer stemness and EMT.

## 2. Materials and methods

### 2.1. Chemicals

Taxifolin, Dichloro (p-cymene) ruthenium(II) dimer were procured from Sigma-Aldrich Chemical Co. anti-rabbit SOX2 (Sex determining region Y-box 2), OCT4 (octamer-binding transcription factor 4), E-cadherin, N-cadherin, PI3K, EGFR (Epidermal growth factor receptor), p53, caspase-3, Akt, mTOR,  $\beta$ -catenin antibodies were procured from GeneTex, Inc (Irvine, CA, USA). DPPH, penicillin, TPTZ, ABTS, foetal bovine serum (FBS), sodium pyruvate, MTT (3-(4, 5 dimethylthiazol-2-yl)-2, 5- diphenyltetrazolium bromide), Annexin V and propidium iodide (PI) (procured from Sigma-Aldrich Chemical Co). All the other reagents were obtained from commercial retail suppliers that were of high purity analytical grade.

### 2.2. Pharmacophore analysis

#### 2.2.1. Protein structure prediction

The overall research is based on the understanding of proteins that are involved in lung cancer. The protein sequences such as PI3K (P42336),  $\beta$ -catenin (CAA61107), EGFR (P00533) were retrieved from UniProt knowledge database. These protein

sequences were used to predict 3D protein structure based on the structural similarity to construct homology models by predicting similar templates using BLASTp.

#### 2.2.2. Ligand preparation and drug likeliness analysis

The compound taxifolin ruthenium-p-cymene complex was designed using ChemSketch 2020.1.1. The chemical structures were saved in .mol format and further used for drug-likeness to understand the druglike properties of the compounds. Pharmacokinetic analysis of the selected compound was predicted using AdmetSAR tool that show high throughput virtual screening based on the traditional medical chemistry properties.

#### 2.2.3. Molecular docking and virtual screening

Based on pharmacophore and pharmacokinetic properties, the selected chemical is further used for molecular docking against target lung cancer proteins. Using AutoDock4.2 and AutoDockVina software to predict the protein–ligand interactions based on binding energy and hydrogen bond formation.

#### 2.3. Synthesis scheme of taxifolin ruthenium-p-cymene complex

The taxifolin ruthenium-p-cymene complex was synthesized by incorporating both taxifolin and ruthenium-p-cymene moiety in a 2:1 ratio at a specific reaction condition. Approximately 60.8 mg (0.2 mmol) of taxifolin was weighed and dissolved in 5 mL of methanol and the pH was maintained at 8 by adding 1 M sodium methoxide solution in methanol. 61.24 mg (0.1 mmol) of ruthenium-p-cymene was dissolved in 15 mL of dichloromethane and the solution was added drop wise to the taxifolin solution with continuous stirring for 24 h in dark condition. Greenish black precipitate of the complex was observed after complete evaporation of the solvent. The precipitate was then collected and washed with ethanol:water (1:1) solution, dried in vacuum dryer and stored at room temperature. The percentage yield of the complex was found to be 94.33%. The complex was soluble in methanol and DMSO. The probable structure of the complex has been depicted in Fig. 1A.

#### 2.4. Characterization

##### 2.4.1. UV–Visible spectroscopy

The UV–visible spectrum of pure taxifolin and taxifolin ruthenium-p-cymene complex was recorded using UV-1900i Shimadzu double beam spectrophotometer.

##### 2.4.2. Job's method

The stoichiometric ratio of taxifolin to ruthenium-p-cymene in the complex was analyzed by continuous variation technique also known as Job's method. Taxifolin of 0.1 mM (1, 2...9 mL) was taken into nine 10 mL volumetric flasks and an aliquot (9, 8...1 mL) of 0.1 mM [Ru(p-cymene) Cl<sub>2</sub>] was added respectively at which a constant mole fraction of solution was attained. All the measurements were made at  $\lambda_{\text{max}}$  which was found to be at 241 nm.

##### 2.4.3. Fourier-transform infrared spectroscopy (FTIR)

FTIR spectrophotometer (IR Affinity-1S, Shimadzu) was used to record the IR spectrum of taxifolin and taxifolin ruthenium-p-cymene complex over the range of 500–4000 cm<sup>-1</sup> wavenumber to distinguish the metal oxide bond as a validation of complexation.

##### 2.4.4. Mass spectroscopy

The molecular weight and the fragmentation pattern of the complex were evaluated by mass spectroscopy using electro-spray ionization mass spectroscopy (ESI-MS) (Xevo G2 Xs Q-ToF ESI Mass).

##### 2.4.5. NMR spectroscopy

The <sup>1</sup>H NMR spectrum of the complex was recorded using Bruker-Avance-600 MHz spectrometer in methanol-D<sub>4</sub>. Tetramethylsilane (TMS) was used as an internal reference.

##### 2.4.6. Scanning electron microscopy

The morphological features of the complex were evaluated using scanning electron microscopy (JEOL MAKE, (UK) Model-JSM-IT800 Schottky Field Emission Scanning Electron Microscope) at an accelerating voltage of 10 kV. The surface characteristics and morphological appearance of the complex was also examined at different magnifications (50X, 4000X, 6000X and 10000X).

##### 2.4.7. X-ray diffractometry

For taxifolin ruthenium-p-cymene complex, no single crystal was formed. To detect the degree of crystallinity of this metal complex, X-ray powder diffraction was carried out. The X-Ray diffraction pattern of the complex was assessed by ULTIMA IV XRD System (Rigaku) operating at 45 kV and 40 mA using CuK $\alpha$  radiation (1.540562 Å) with the Bragg-Brentano geometry with step size 0.02 (2 $\theta$ ), step time 3 sec from 5 to 95. The average size of the crystallites has also been estimated using the Scherrer's equation;

$$D = K\lambda/\beta \cos\theta$$

Where, D represents average crystallite size, K is Scherrer constant,  $\lambda$  represents X-ray wavelength,  $\beta$  is line broadening FWHM (full width half maxima) in radians,  $\theta$  is Bragg's angle in degree. FWHM has been calculated based on Single Line profile Analysis using X'pert Organizer (PANalytical) software.

#### 2.5. In vitro antioxidant assay

##### 2.5.1. DPPH assay

The DPPH assay was performed as per the method of Rahman and co researchers (Rahman et al., 2015). The absorbance of test solutions was measured at 517 nm for both taxifolin and taxifolin ruthenium-p-cymene complex, in which 0.1 mM DPPH solution was considered as control. The % of radical scavenging activity (% RSA) was calculated as

$$\%RSA = \{(A_0 - A_1)/A_0\} \times 100\%$$



cell viability was observed at 48 h. The cell viability was investigated through mitochondrial succinate dehydrogenase which metabolizes MTT to produce formazan crystals. % Cell viability was measured as:

$$\% \text{Cell viability} = [\text{Mean absorbance of treated cells} / \text{Mean absorbance of Untreated cells}] \times 100$$

The  $IC_{50}$  (Half-maximal inhibitory concentration) value was determined by using linear regression equation i.e.,  $y = mx + C$ , where,  $y = 50$ ,  $m$  and  $C$  values were derived from the viability graph.

#### 2.7.3. Assessment of olegonucleosomal fragmentation

The effect of the complex on the cancer cells was observed by staining the cells with fluorescent nuclear dye 4',6-diamidino-2-phenylindole dihydrochloride (DAPI). The cells were observed under ZEISS LSM 880 Fluorescence live cell imaging system (Confocal Microscopy) with filter cube with Excitation 358 nm and Emission 461 nm. Images were analysed by ZEN Blue Software and recorded.

#### 2.7.4. Colony formation assay

The effect of the complex on the cancer cell proliferation and colony formation was evaluated by clonogenic assay after 48 h of incubation. The colonies of the cancer cells were stained with 0.5% crystal violet solution and visually quantified to distinguish the colonies which comprises > 50 cells/colony. The clonogenicity was then evaluated by using the formula below:

$$\text{Clonogenicity} = (\text{Cloning number} / 500x) \times 100$$

The experiment was conducted in triplicate manner.

#### 2.7.5. Transwell migration assay

The cell invasion activity of the A549 and NCI-H460 cell lines were assessed by transwell migration assay. The cells were seeded ( $5 \times 10^4$  cells/well) in the upper chamber of the transwell and supplemented with 0.1% FBS containing DMEM medium. The lower chamber was filled with DMEM, supplemented with 10% FBS. The cells of both chambers were treated with different concentrations of the complex. After 48 h of incubation the cells in the lower chamber was fixed by 4% paraformaldehyde and stained with 0.25% crystal violet. The wells were then scanned at four random fields and the numbers of invaded cells were counted using bright field microscope at 40X magnification.

#### 2.7.6. Sphere formation assay

A549 and NCI-H460 cells were seeded in the ultra-low attachment multiwall plate at the concentration of  $1 \times 10^4$  cells/ml in 3dGRO spheroid medium. The cells were treated with various concentrations ( $IC_{25}$ ,  $IC_{50}$ , and  $IC_{75}$ ) of complex and incubated for 10 days at 37 °C in 5%  $CO_2$ . Then the pictures of the spheres were taken and the sphere numbers were counted in four random fields under the microscope.

#### 2.7.7. Flow cytometry

The apoptosis assay and cell cycle distribution analysis were performed on the A549 and NCI-H460 cells after the treatment with the complex through flow cytometric analysis. The cells were suspended and the nuclear DNA was tagged with

Annexin-V conjugated-FITC and propidium iodide (PI). Acquisition was done by using BD FACSCalibur and data were analysed by BD Cell Quest Pro Software (Version: 6.0).

#### 2.7.8. Detection of caspase-3 expression

The expression of caspase-3 in A549 and NCI-H460 cells were investigated by flow cytometry. The cells were seeded in 6 well plate and treated with different concentrations ( $IC_{25}$ ,  $IC_{50}$ , and  $IC_{75}$ ) of the complex for 48 h. The cells were then treated with anti-rabbit caspase-3 polyclonal antibody at 37 °C in dark environment. The percentage of cells labeled with caspase-3 antibody was investigated by flow cytometric analysis.

#### 2.7.9. Western blot

The expression of PI3K, EGFR, SOX2, OCT4, N-cadherin, E-cadherin on the A549 and NCI-H460 cells was detected by using the western blot analysis. The cells were treated with different concentrations ( $IC_{25}$ ,  $IC_{50}$ , and  $IC_{75}$ ) of the complex and incubated for 48 h. The total cell lysate from each group was obtained that was further resolved in SDS-PAGE (8–12%) electrophoresis and transferred to PVDF membrane. The membrane was then blocked with 5% non-fat dried milk in PBST and incubated with anti-rabbit PI3K, EGFR, SOX2, OCT4, N-cadherin and E-cadherin antibodies (1:500 dilution) overnight in humidified chamber. After incubation the membrane was treated with HRP conjugated goat anti-rabbit secondary antibodies and the expression was detected by chemiluminescent (ECL Western Blotting) kit with  $\beta$ -actin as loading control.

### 2.8. In vivo study

#### 2.8.1. Animal

For the toxicity study Swiss albino mice (15–20 g), 6–8 weeks old of both sexes (females should be nulliparous and nonpregnant) and for chemotherapeutic study 6 weeks old male Balb/c mice (20–30 g) were purchased from registered animal breeder (Regd.no. –1458/PO/E/S/11/CPCSEA Dated- 12.05.2011). The animals were placed in polypropylene cages in 12 h light/dark cycle at 22 °C ( $\pm 3^\circ\text{C}$ ) with relative humidity of about 50–58%. Animals were given free access to food and demineralized water. The experimental protocol was approved by the Institutional Animal Ethics Committee and by the Animal Regulatory Body of the Government (1458/PO/E/S/11/CPCSEA dated 12.05.2011) and experiments have been conducted in accordance to ARRIVE guidelines. The animals were acclimatized to the laboratory condition for one week prior to the initiation of the experiment.

#### 2.8.2. Toxicity study

The toxicity study has been demonstrated in [Supplementary file 1](#).

#### 2.8.3. Experimental protocol

After the acclimatization period, the animals were randomly distributed into seven groups (I, II, III, IV, V, VI, VII) and each group consist of six animals. When the mice were 7–8 weeks old, all the animals (except group I) were given a single

i.p. injection of 100 mg/kg Benzo( $\alpha$ ) pyrene in 0.2 mL of corn oil to induce the lung cancer. Treatment with taxifolin ruthenium-p-cymene complex was started after 2 weeks of benzo( $\alpha$ )pyrene (B( $\alpha$ )P) induction and continued for 20 weeks. The experimental design is followed as:

Group I- Normal untreated vehicle control animals, Group II- B( $\alpha$ )P treated animals assigned as carcinogen control, Group III- B( $\alpha$ )P treated animals receives 50 mg/kg complex, Group IV- B( $\alpha$ )P treated animals receives 100 mg/kg complex, Group V- B( $\alpha$ )P treated animals receives 200 mg/kg complex, Group VI- B( $\alpha$ )P treated animals receives 50 mg/kg taxifolin, Group VII- B( $\alpha$ )P treated animals receives 50 mg/kg ruthenium-p-cymene.

The tumor volume was assessed via caliper two times per week and tumor sizes were calculated by using the following equation (Dethlefsen et al., 1968):

$$\text{Tumor volume (V)} = \pi/6 \times (\text{length}) \times (\text{width})^2$$

The tumor volume and body weight were assessed two times per week over the course of the treatment. At the end of the experiment the animals were sacrificed using pentobarbital sodium. The lungs were excised, fixed in formalin, transferred to 70% alcohol, and examined for further experimentations.

#### 2.8.4. Histopathology of lungs

An initial incision was made at the ventral midline which extends from the chin to the pubis. The sub cutis of the ventral and lateral thorax and abdomen was completely exposed. Subsequently, the rib cage was removed and the entire thoracic cavity was exposed. Then all dorsal attachments were cut and the tongue, esophagus, trachea, heart, and lungs were removed from the thoracic cavity. Heart and the other organs were separated from trachea and lungs and the whole tissue was fixed into 10% neutral buffered formalin (NBF) solution for 24 h. The excised tissues were dehydrated and embedded in paraffin wax. The tissues of 5  $\mu$ m thickness were kept on slides and rehydrated by graded alcohol. The slides were stained using haematoxylin and eosin (H&E), which were observed under the light microscope for histological evaluation.

#### 2.8.5. Antioxidant assay of lung

The in vivo antioxidant assay has been depicted in [Supplementary file 1](#).

#### 2.8.6. Immunohistochemistry

The excised lung tissues, mounted on poly-L-lysine coated glass slides were deparaffinized and treated with 3% H<sub>2</sub>O<sub>2</sub>. The blocking solution was added to the slides and then incubated with appropriately diluted (1:500) primary antibodies (anti-rabbit p53, Akt, mTOR, caspase-3,  $\beta$ -catenin) overnight at 4 °C in a humidified chamber. After incubation, the HRP conjugated goat anti-rabbit secondary antibodies were added to the slides for 2 h. The nuclear staining was done by DAB and hematoxylin was utilized for background staining. The slides were then observed under light microscope and the immune-positive cells were quantified by ImageJ software (version 1.8.0).

#### 2.8.7. Cell proliferation assay

The excised lung tissues, mounted on poly-L-lysine coated glass slides were deparaffinized and treated with 3% H<sub>2</sub>O<sub>2</sub>. The blocking solution was added to the slides and then incubated with appropriately diluted (1:500) anti-rabbit Ki-67 antibody overnight at 4 °C. The slides were then treated with HRP conjugated goat anti-rabbit secondary antibody for 2 h. The nuclear staining was done by DAB and hematoxylin was used for background staining. The Ki-67 expression was examined under light microscope and the immune-positive cells were quantified by ImageJ software (version 1.8.0).

#### 2.8.8. Apoptosis assay by TUNEL method

The occurrence of apoptotic events in the lung was assessed by TUNEL (Terminal deoxynucleotidyl transferase dUTP Nick-End Labeling) assay. The proteinase-K solution was added to the tissue sections and further treated with H<sub>2</sub>O<sub>2</sub> to abrogate the peroxidase activity. poly-L-lysine coated slides of colon tissues were used for TUNEL assay. The slides were treated with proteinase-K followed by H<sub>2</sub>O<sub>2</sub> to block activity of endogenous peroxidase. The tissue sections were supplemented with terminal deoxynucleotidyl transferase (TdT) accompanied by TdT and dUTP containing TdT reaction at 37 °C for an hour. Later on, saline citrate was added to abort. The slides were further incubated antidigoxigenin peroxidase (1:1000) at 37 °C for half an hour and finally stained with DAB and hematoxylin. The slides were then observed under microscope followed by quantification of the TUNEL-positive cells.

The labeling index (LI) designated the percentage of Ki-67-positive cells. The apoptotic index (AI) represented the percentage of TUNEL-positive cells to the total number of cells.

#### 2.9. Statistical analysis

Data were expressed as the mean  $\pm$  SEM. All the statistical evaluation was done by ANOVA followed by Tukey's post hoc multiple comparison test using Graph Pad Prism (Version 5). The differences were found to be statistically significant when  $p < 0.05$ .

### 3. Results

#### 3.1. Pharmacophore analysis

##### 3.1.1. Bioactive properties

The bioactive properties of the complex was predicted based on the probable activity against different target receptors

**Table 1** Bioactive properties.

Properties	complex
GPCR Ligand	0.14
Ion channel modulator	0.04
Kinase inhibitor	0.02
Nuclear receptor ligand	0.29
Protease inhibitor	0.05
Enzyme inhibitor	0.15

(GPCR ligand, Ion channel modulator, Kinase inhibitor, Nuclear receptor ligand, Protease inhibitor and Enzyme inhibitor) (Table 1) and the results showed the increasing positive values which represents the best active potential against target receptors. The complex showed highest positive value for nuclear receptor ligand (0.29) suggesting great binding affinity to the DNA.

### 3.1.2. Pharmacokinetic profile

The pharmacokinetic profile of the complex has been documented in the Tables 2, 3. According to the ADMET profile, the complex is a P-glycoprotein substrate and showed a great absorption from GI tract and through blood–brain-barrier. The toxicity profile of the complex reported that the complex is not carcinogenic but having high fish toxicity and honey bee toxicity probability. It is also non AMES toxic and having grade III acute oral toxicity i.e. slightly toxic and slightly irritating.

### 3.1.3. Molecular docking

Docking interaction of proteins with ligand molecules exhibited that lung cancer proteins such as PI3K,  $\beta$ -catenin and EGFR were strongly interacted with Taxifolin ruthenium-p-cymene complex (Table 4). The PI3K and EGFR protein structure were forming 4 hydrogen bonds with the interaction energy of  $-7.2$  and  $-6.9$  kcal/mol respectively within active site of amino acids such as Ser753, Glu849, Arg852 and Glu738, Met769, Gly772 respectively.  $\beta$ -catenin was forming 3 hydrogen bonds with the energy of  $-7.2$  kcal/mol within active site of amino acids Arg474, Arg515 and Tyr654 (Fig. 1B, C, D).

## 3.2. Instrumental analysis

### 3.2.1. UV–Visible spectroscopy

The absorption spectra of taxifolin represent two characteristics absorption band at 287 nm and 224 nm for band I and

**Table 2** ADMET predicted profile- classification.

Model	Result	Probability
<b>Absorption</b>		
Blood-brain barrier	BBB (+)	0.6006
Human intestinal absorption	HIA (+)	0.8420
Caco-2 permeability	Caco-2 (-)	0.5353
P-glycoprotein substrate	Substrate	0.5643
<b>Distribution</b>		
Sub-cellular localization	Mitochondria	0.6004
<b>Metabolism</b>		
CYP450 3A4 substrate	Substrate	0.5841
CYP450 2D6 substrate	Non- substrate	0.8066
CYP450 2C9 substrate	Non- substrate	0.7982
<b>Toxicity</b>		
AMES toxicity	Non AMES toxic	0.7740
Carcinogens	Non-carcinogens	0.7749
Fish toxicity	High FHMT	0.9946
Honey bee toxicity	High HBT	0.6639
Biodegradation	Not ready biodegradable	0.9911
Acute oral toxicity	III	0.4393

**Table 3** ADMET predicted profile- Regression.

Model	Value	Unit
<b>Absorption</b>		
Aqueous solubility	$-4.8495$	LogS
Plasma protein binding	1.096	100%
<b>Toxicity</b>		
Rat acute toxicity	2.7894	LD <sub>50</sub> , mol/kg
Fish toxicity	0.4825	pLC50, mg/L

**Table 4** Molecular docking.

Proteins	H-Bonds	Bond Energy	Amino Acids
PI3K	4	$-7.2$	Ser753, Glu849, Arg852,
$\beta$ -catenin	3	$-7.2$	Arg474, Arg515, Tyr654,
EGFR	4	$-6.9$	Glu738, Met769, Gly772

band II respectively. The absorption spectra of the taxifolin ruthenium-p-cymene complex showed significant shifts in their absorption band position (Fig. 2A). The band I shift from 287 nm to 295 nm and band II shifts from 224 nm to 227 nm. The occurrence of the maximum shift occurs for band I position (Fig. 2B).

### 3.2.2. Job's method

The interaction between taxifolin and ruthenium-p-cymene dimer molecule has been evaluated by spectrophotometric analysis through Job's method. The solution containing taxifolin and ruthenium-p-cymene dimer at a ratio of 1:1.5 or approximately 1:2 at a pH of 6.8 shows the maximum absorbance (0.854) (Fig. 2C).

### 3.2.3. FTIR study

The FTIR spectra of taxifolin and taxifolin ruthenium-p-cymene complex have been depicted in (Fig. 2D) and evaluated Table 5. A distinguishable peak at the region of  $628.6\text{ cm}^{-1}$  has been appeared in the IR spectra of the complex that is absent in the IR spectrum of taxifolin. This peak corresponds to the (Ru-O) bond due to the complex formation. The appearance of  $\nu$  (O–H) band at  $3440.03\text{ cm}^{-1}$  for taxifolin is shifted to  $3451.19\text{ cm}^{-1}$  for the complex. The  $\nu$  (C=O) stretching band is shifted from  $1621.41\text{ cm}^{-1}$  to  $1634.64\text{ cm}^{-1}$ .

### 3.2.4. Mass spectroscopy

The mass spectrum of taxifolin ruthenium-p-cymene complex is depicted in (Fig. 3A). The highest molecular abundance was observed for the molecular ion peak with  $m/z$  value 573.0148. The other peaks that appeared in the mass spectrum were due to the fragmentation. The mechanism of the fragmentation has shown in the (Fig. 3B).

### 3.2.5. NMR spectroscopy

6.96 (d, 1H,  $J = 1.8$  Hz); 6.85 (dd, 1H,  $J = 7.8, 1.8$  Hz); 6.8 (d, 1H,  $J = 7.8$  Hz); 5.92 (d, 1H,  $J = 1.8$  Hz); 5.89 (d, 1H,  $J = 2.4$  Hz); 5.87 (d, 2H,  $J = 6$  Hz); 5.64 (d, 2H,

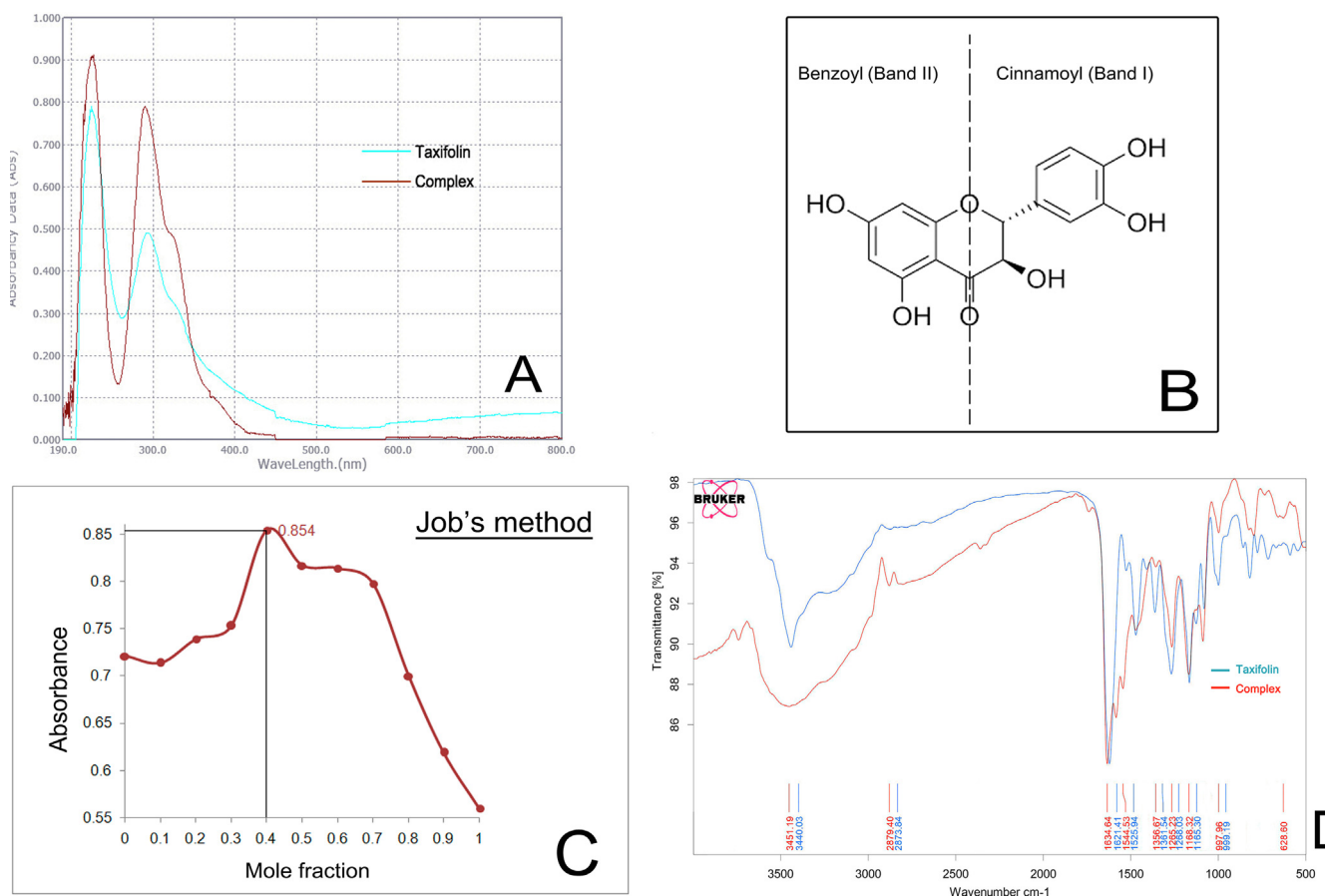


**Fig. 2** (A) UV-visible spectra of taxifolin and taxifolin ruthenium-p-cymene complex (B) taxifolin and its different bands (I and II) related to UV-vis spectroscopy (C) Plot of absorbance vs. mole fraction of taxifolin at 241 nm (D) FTIR spectra of taxifolin and taxifolin ruthenium-p-cymene complex.

**Table 5** IR spectra of the taxifolin and the complex (band position in cm<sup>-1</sup>).

Compound	$\nu$ (O—H)	$\nu$ (C=O)	$\nu$ (C=C)	$\nu$ (C—OH)	$\nu$ (C—O—C)	$\nu$ (M—O)
Taxifolin	3440.03	1621.41	1470.88	1268.03	1165.3	—
Complex	3451.19	1634.64	1471.69	1265.23	1168.32	628.6

$J = 6$  Hz); 5.62 (d, 2H,  $J = 4.8$  Hz); 5.49 (s, 1H); 5.42 (d, 1H,  $J = 5.4$  Hz); 4.92 (d, 1H); 4.51 (d, 1H,  $J = 11.4$  Hz); 2.77 (m, 1H); 2.19 (s, 3H); 1.21 (d, 6H). (Fig. 3C) depicted the <sup>1</sup>H NMR spectrum of the taxifolin ruthenium-p-cymene complex.

### 3.2.6. Scanning electron microscopy

The surface morphology of the complex is evaluated by scanning electron microscopy with various magnifications (50X, 4000X, 6000X and 10000X) which has been demonstrated in the (Fig. 4 A-D). The orthorhombic crystal structure of the complex can be clearly visualized from the SEM images with sharp edges and symmetrical structures.

### 3.2.7. X-ray diffractometry

X-ray Diffractogram of taxifolin ruthenium-p-cymene complex has been depicted in Fig. 4E. The X-ray Diffractogram of the complex exhibited three major high intensity peaks at three diffraction angles which include 31.74°, 45.51° and

56.54° with its relative intensity 100%, 74.35%, and 19.81% respectively. The maximum intensity was found at 31.74° and minimum intensity was recorded at 71.53°. The interplanar spacing (d) as well as their relative intensities in relation to acquired peaks at different diffraction angles has been depicted in Table 6. The crystallite sizes for the major three peaks have been recorded in Table 6. The average crystallite size of taxifolin ruthenium-p-cymene complex was found to be 49.81 nm.

## 3.3. Evaluation of antioxidant status

### 3.3.1. DPPH activity

The absorption spectra of different DPPH solution containing different concentration of free taxifolin and the complex has been depicted in (Fig. 5A). The % radical scavenging activity (% RSA) of free taxifolin increases very slightly with increasing concentration and the maximum % RSA



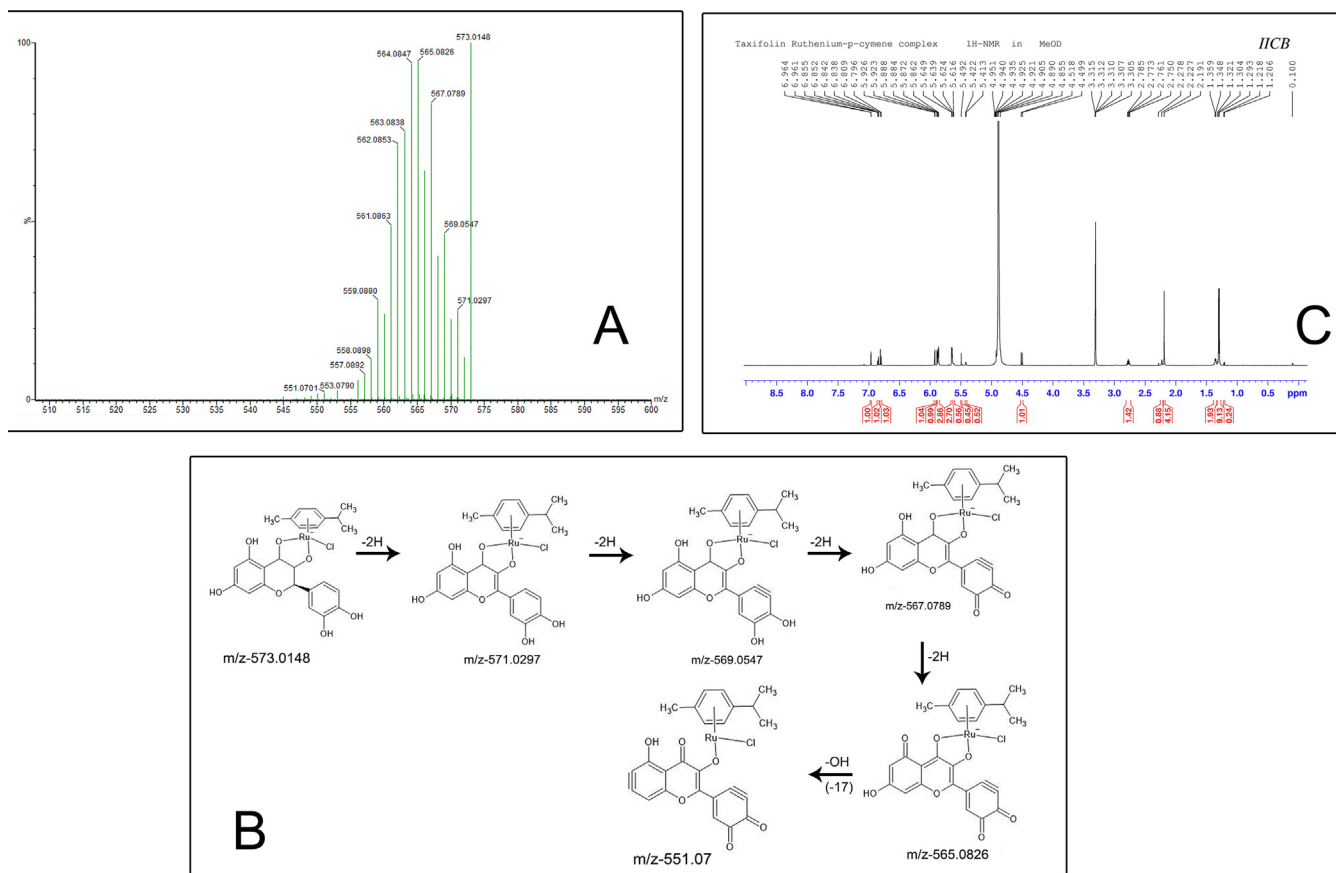


**Fig. 3** (A) Mass spectroscopy of taxifolin ruthenium-p-cymene complex (B) The fragmentation mechanism of the complex (C)  $^1\text{H}$  NMR spectra of taxifolin ruthenium-p-cymene complex.

was detected to be 99.23%. But for the complex it showed a drastic increase in the % RSA with increasing concentration which reaches up to 98.85%. The complex shows less DPPH radical scavenging activity than the free taxifolin at same concentration.

### 3.3.2. ABTS activity

The ABTS assay of taxifolin and the complex has been depicted in the (Fig. 5B). It was found that the absorbance of ABTS solution decreases with increase in the concentration of the complex. Along with that the complex showed more radical scavenging activity than that of free taxifolin.

### 3.3.3. FRAP activity

The absorbance of free taxifolin and the complex of different concentrations have been estimated at 593 nm wavelength in presence of  $\text{Fe}^{3+}$ -TPTZ. The complex exhibited enhanced antioxidant capacity than free taxifolin which has been depicted in the (Fig. 5C).

## 3.4. In vitro study

### 3.4.1. Induction of cytotoxicity through taxifolin ruthenium-p-cymene complex treatment

Taxifolin ruthenium-p-cymene complex inhibits the cell viability of A549 and NCI-H460 lung cancer cell lines in a dose dependent manner (Fig. 6A, B). The cell viability of A549

was found to be 91.28%, 72.35%, 49.82%, 32.98%, 13.52% and for NCI-H460 the cell viability was 76.25%, 51.64%, 34.75%, 20.88%, 12.10% at the concentrations of 43.6, 87.3, 174.5, 349, 698.1  $\mu\text{M}$  respectively. From the above experiment the  $\text{IC}_{50}$  value of the complex was calculated as 187.19  $\mu\text{M}$  and 108.62  $\mu\text{M}$  for A549 and NCI-H460 cell lines respectively. For chemotherapeutic study, the working concentrations of the complex were determined as  $\text{IC}_{25}$ ,  $\text{IC}_{50}$  and  $\text{IC}_{75}$ . The  $\text{IC}_{25}$ ,  $\text{IC}_{50}$  and  $\text{IC}_{75}$  values for A549 was 93.6  $\mu\text{M}$ , 187.19  $\mu\text{M}$ , 280.78  $\mu\text{M}$  and for NCI-H460 cell lines the values were 54.31  $\mu\text{M}$ , 108.62  $\mu\text{M}$ , 162.93  $\mu\text{M}$  respectively.

### 3.4.2. Taxifolin ruthenium-p-cymene complex caused nuclear fragmentation

Taxifolin ruthenium-p-cymene complex induced nuclear fragmentation and membrane blebbing in A549 and NCI-H460 cell line (Fig. 6C, D). The maximum nuclear condensation was observed at the concentration of 280.78  $\mu\text{M}$  and 162.93  $\mu\text{M}$  in A549 and NCI-H460 cell line respectively.

### 3.4.3. Taxifolin ruthenium-p-cymene complex inhibited cellular proliferation

The treatment with the complex significantly inhibited the colony formation in both A549 and NCI-H460 cell lines (Fig. 6E). The cells treated with the complex exhibited the inhibition of colony number (Fig. 6F, I), colony size (Fig. 6G, J) and plating efficiency (PE) (Fig. 6H, K) as compared to the untreated cells in both the cell lines respectively. In comparison to the

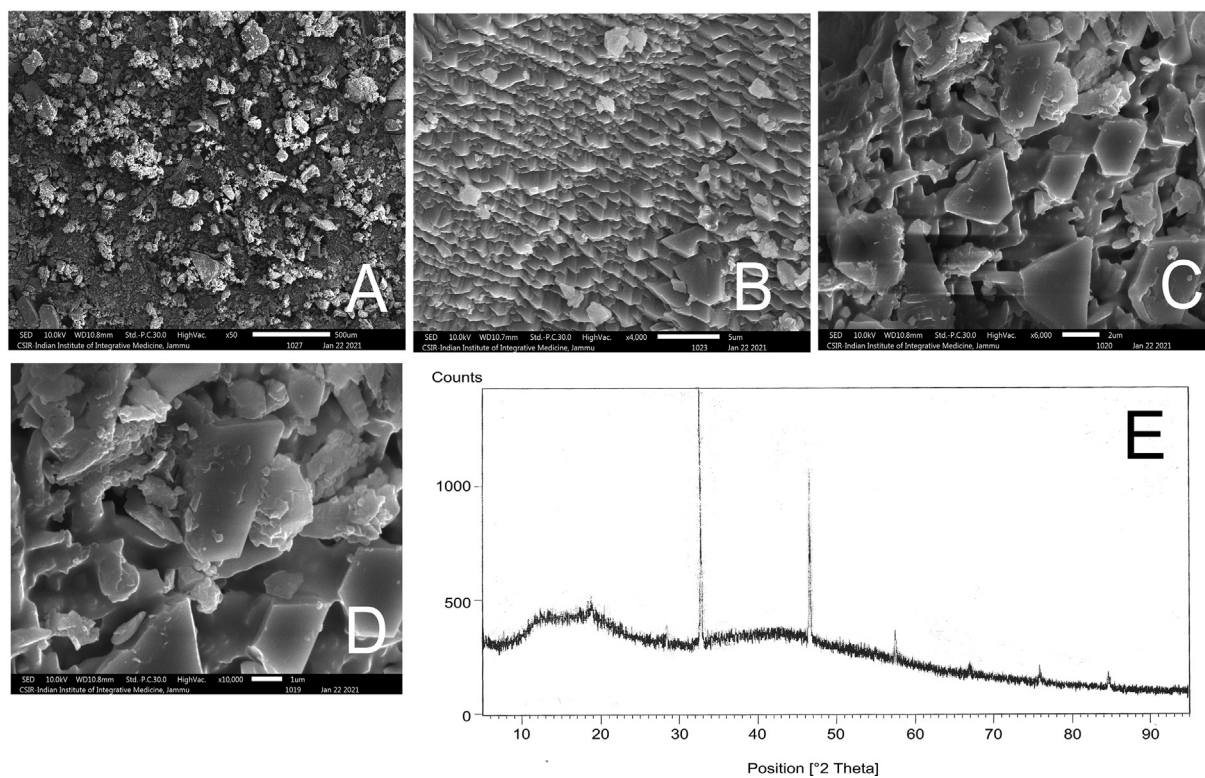


**Fig. 4** Scanning electron microscopy (SEM) of the complex at (A) 50X (B) 4000X (C) 6000X (D) 10000X. (E) X-ray diffractogram of taxifolin ruthenium-p-cymene complex.

**Table 6** X-ray diffraction data of taxifolin ruthenium-p-cymene complex.

Position (2 $\theta$ )	d-spacing (Å)	Relative intensity (%)	$\beta$ (FWHM)	D (crystallite size) (nm)	D average (nm)
11.6903	7.57007	7.57			49.81142613
18.0346	4.91880	11.20			
27.3791	3.25756	14.09			
31.7384	2.81938	100.00	0.1436	56.8531084	
45.5110	1.99312	74.35	0.1464	58.16800806	
56.5396	1.62774	19.81	0.2591	34.41316194	
66.2920	1.40997	6.62			
71.5309	1.31904	1.61			
75.3766	1.26101	8.16			
84.0554	1.15153	8.44			

untreated cells the complex treated cells displayed lowest PE at the concentrations of 280.78  $\mu$ M and 162.93  $\mu$ M in A549 and NCI-H460 cell lines respectively.

#### 3.4.4. Taxifolin ruthenium-p-cymene complex inhibited EMT

Taxifolin ruthenium-p-cymene complex treatment inhibited the invasive cells in both A549 and NCI-H460 cell lines (Fig. 7A, B) in a dose dependent manner. The western blot analysis (Fig. 7C) further confirmed the inhibition of EMT through the downregulation and upregulation of N-cadherin and E-cadherin expression respectively in both the cell lines.

#### 3.4.5. Taxifolin ruthenium-p-cymene complex inhibited stemness

Taxifolin ruthenium-p-cymene complex treated cells exhibited dose dependent inhibition of sphere formation (Fig. 7D) in

respect to both the diameters of spheres (Fig. 7E) and number of spheres per 200 cells (Fig. 7F) in both the cell lines. In addition, the expressions of stem cell markers such as SOX2 and OCT4 were also investigated in both the cell lines through western blotting (Fig. 7G). The western blot analysis depicted marked downregulation in the expression of SOX2 and OCT4 followed by the complex treatment in both the cell lines.

#### 3.4.6. Taxifolin ruthenium-p-cymene complex induce apoptosis and cell cycle arrest

The induction of apoptosis in A549 and NCI-H460 cell line due to the treatment with the complex for 48 h has been demonstrated in Fig. 8A and Fig. 9A respectively. The total percentage of apoptotic cells in A549 cells was found to be 90.87%, 92.42%, 97.07% and for NCI-H460 cells it was 33.28%, 42.87%, 82.62% at the concentration of IC<sub>25</sub>, IC<sub>50</sub>

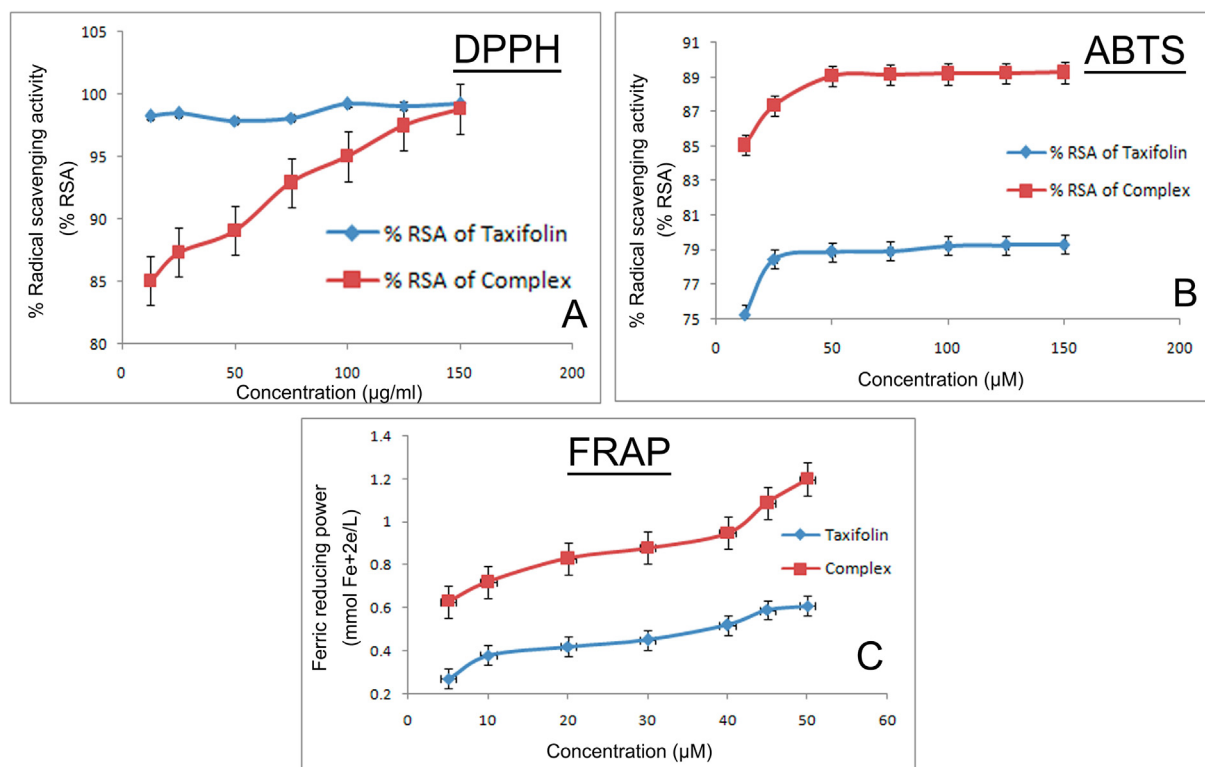


**Fig. 5** Measurement of antioxidant potential of the complex by (A) DPPH method (B) ABTS method (C) FRAP method.

and  $IC_{75}$  of the complex respectively (Fig. 8B, 9B). The percentage of early apoptosis and late apoptosis was increased dose dependently in both the cell lines followed by the treatment with complex for 48 h (Fig. 8C, D and Fig. 9C, D). A significant decrease in the percentage of live cells was noted in the complex treated cells (Fig. 8E, 9E). The percentage of dead cells was also evaluated in the complex treated cells. The  $IC_{50}$  of the complex exhibited maximum percentage of dead cells in both the cell lines (Fig. 8F, Fig. 9F).

The distribution of cell cycle phases on untreated cells and complex treated cells in both the cell lines have been depicted in Fig. 8G, H and Fig. 9G, H. In A549 cell line, the cell cycle analysis subjected to sub G0/G1 phase (apoptotic phase) demonstrated that 1.46%, 6.09%, 13.97% and 9.61% of cell got arrested in untreated,  $IC_{25}$ ,  $IC_{50}$  and  $IC_{75}$  group respectively. Similarly, in G0/G1 phase (growth Phase), 66.37%, 60.76%, 51.5% and 40.71% of cells, in S phase (synthetic phase), 3.79%, 6.99%, 4.68% and 13.6% of cells, in G2/M phase, 22.76%, 24.78%, 27.85% and 34.07% of cells got arrested in untreated,  $IC_{25}$ ,  $IC_{50}$  and  $IC_{75}$  group respectively (Fig. 8G, H). In NCI-H460 cell line, the cell cycle analysis subjected to sub G0/G1 phase (apoptotic phase) demonstrated that 1.93%, 4.84%, 12.01% and 21.27% of cells got arrested in untreated,  $IC_{25}$ ,  $IC_{50}$  and  $IC_{75}$  group respectively. Similarly, in G0/G1 phase (growth Phase), 70.69%, 57.55%, 47.56% and 30.41% of cells, in S phase (synthetic phase), 1.94%, 10.08%, 12% and 2.83% of cells, in G2/M phase, 20.72%, 24.44%, 27.36% and 42.29% of cells got arrested in untreated,  $IC_{25}$ ,  $IC_{50}$  and  $IC_{75}$  group respectively (Fig. 9G, H).

### 3.4.7. Taxifolin ruthenium-p-cymene complex increased caspase-3 expression

The expression of caspase-3 in A549 and NCI-H460 cell line followed by the treatment with various concentration of taxifolin ruthenium-p-cymene complex for 48 h has been demonstrated in Fig. 10A, B respectively. The untreated group exhibited highest number of caspase-3 labeled cells in M1 quadrant. Whereas, the number of caspase-3 labeled cells in M2 quadrant was significantly increased followed by the drug treatment in both the cell lines.

### 3.4.8. Effect of taxifolin ruthenium-p-cymene complex on the expression of PI3K, EGFR

The western blot analysis demonstrated that the treatment with the complex significantly inhibited the expression of PI3K and EGFR in the both A549 and NCI-H460 cell line as compared to the untreated cells (Fig. 10C).

## 3.5. In vivo carcinogenic study

### 3.5.1. Taxifolin ruthenium-p-cymene rehabilitates carcinogenicity and reduces tumor burden

The histopathological alterations of lung at the end of chemotherapeutic study have been depicted in Fig. 11. The normal control group (Fig. 11A) exhibited the normal morphological architecture of lungs which includes bronchiole (b), pulmonary alveoli (pa), alveolar sac (as), blood vessels (bv), pulmonary capillary (pc), columnar epithelium (ce), smooth muscle (sm). The carcinogen control group

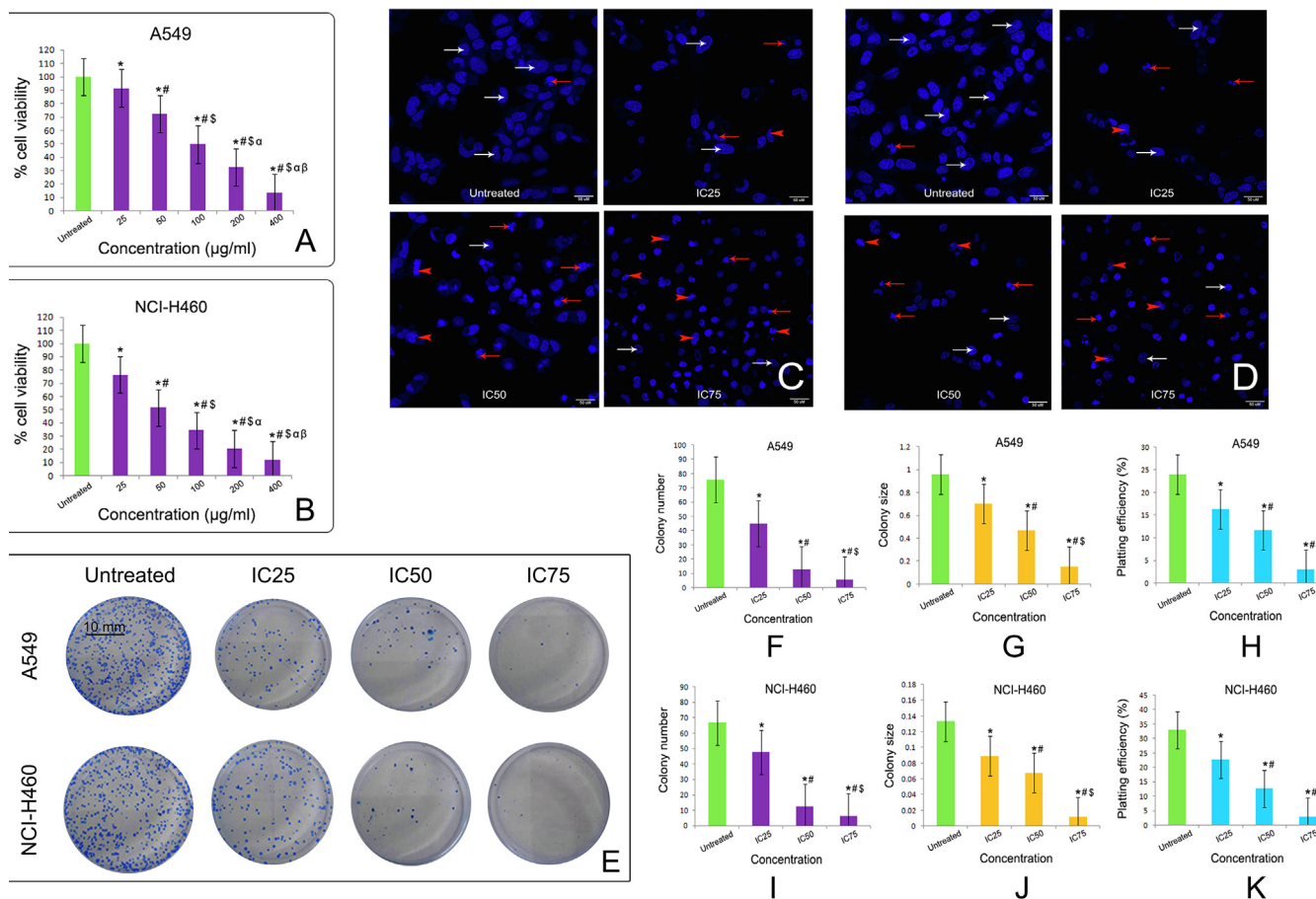


**Fig. 6** Effect of taxifolin ruthenium-p-cymene complex on the cell viability of (A) A549 cells and (B) NCI-H460 cells at 48 h of incubation. \* represented  $p < 0.05$  as compared to untreated cells. Similarly, # represented  $p < 0.05$  as compared to 25  $\mu\text{g/ml}$  concentration, \$ represented  $p < 0.05$  as compared to 50  $\mu\text{g/ml}$  concentration,  $\alpha$  represented  $p < 0.05$  as compared to 100  $\mu\text{g/ml}$  concentration and  $\beta$  represented  $p < 0.05$  as compared to 200  $\mu\text{g/ml}$  concentration. DAPI staining of (C) A549 cells and (D) NCI-H460 cells after 48 h of taxifolin ruthenium-p-cymene complex treatment denoting viable cells (white arrows), nuclear fragmentations (red arrows) and membrane blebbing (red arrowheads). (E) Clonogenic assay of A549 and NCI-H460 cells after 48 h of treatment with taxifolin ruthenium-p-cymene complex. Quantification of (F) colony number, (G) colony size, and (H) plating efficiency for A549 cells. Quantification of (I) colony number, (J) colony size, and (K) plating efficiency for NCI-H460 cells. \* represented  $p < 0.05$  as compared to untreated cells. Similarly, # represented  $p < 0.05$  as compared to IC<sub>25</sub>, \$ represented  $p < 0.05$  as compared to IC<sub>50</sub>. Quantification of colony number and size was performed using Image J public domain software. Data represented as means  $\pm$  SEM from different experiments in triplicate. The results were compared using ANOVA, followed by a Tukey's multiple comparison post-hoc analysis.

(Fig. 11B) showed thickened alveolar walls (*t*), congested alveolar cavity (*cac*), nodular lymphocytic collection (*nlc*), lymphocyte infiltration (*li*) in alveolar space, severe fibrosis (*f*) and formation of granuloma (*g*). On the other hand, taxifolin ruthenium-p-cymene treated group (Fig. 11C-E) restored the normal cellular architecture of the lung tissue. Though slight lymphocyte infiltration (*li*) and minor thickening of alveolar walls (*t*) were observed in 100 mg/kg group (Fig. 11D). The 200 mg/kg group (Fig. 11E) did not show any alterations in the B( $\alpha$ )P induced lung and successfully restored the morphological features of healthy lung. Whereas, 50 mg/kg taxifolin treated group (Fig. 11F) showed lymphocyte infiltration (*li*) in alveolar space, thickened alveolar walls (*t*) and congested alveolar cavity (*cac*). 50 mg/kg ruthenium-p-cymene treated group (Fig. 11G) demonstrated thickened alveolar walls (*t*), congested alveolar cavity (*cac*), nodular lymphocytic collection (*nlc*) and lymphocyte infiltration (*li*) in alveolar space. In addition,

200 mg/kg taxifolin ruthenium-p-cymene treatment significantly ( $p < 0.05$ ) reduces the tumor volume and tumor weight as compared to the carcinogen control group (Fig. 11H, I).

### 3.5.2. Effect of taxifolin ruthenium-p-cymene complex on the expression of p53, caspase-3, Akt, mTOR and $\beta$ -catenin

Fig. 12 and Table 7 depicted the expression profiling of p53, caspase-3, Akt, mTOR and  $\beta$ -catenin on the cancerous lung tissue of mice. A significantly low expression of p53 and caspase-3 was noted in the carcinogen control group (Fig. 12(i)B, (ii)B) in comparison to the normal control (Fig. 12(i)A, (ii)A) ( $p < 0.05$ ). Whereas, a dose dependent increase in the expression of p53 and caspase-3 was exhibited in the complex treated group (Fig. 12(i) C-E, (ii) C-E). The 200 mg/kg group (Fig. 12(i)E, (ii)E) showed significant expression of p53 and caspase-3 on the alveolar wall and bronchiolar epithelial

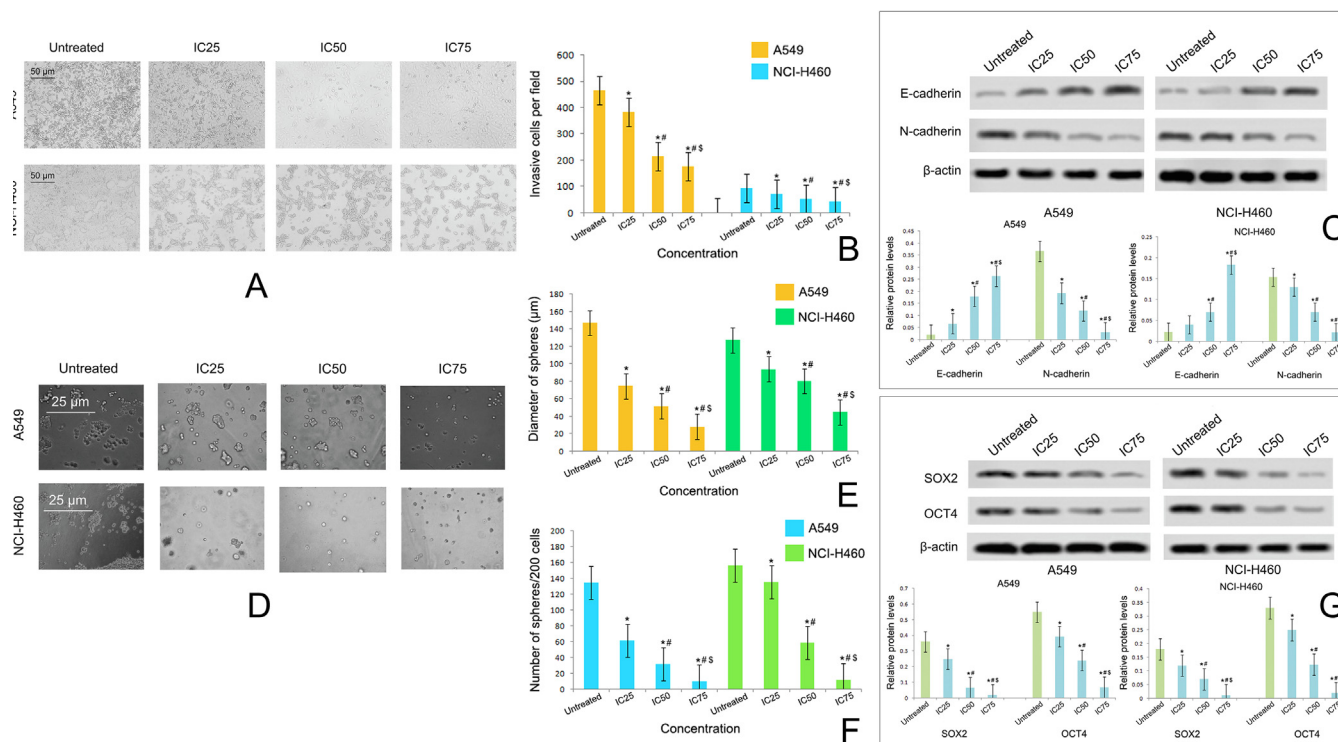


**Fig. 7** (A) Effect of taxifolin ruthenium-p-cymene complex on the invasion of A549 and NCI-H460 cells at 48 h of incubation (B) Estimation of invasive cells per field (C) Western blot analysis of E-cadherin and N-cadherin on A549 and NCI-H460 cells (D) Effect of taxifolin ruthenium-p-cymene complex on the sphere formation of A549 and NCI-H460 cells at 10 days of incubation (E) Estimation of sphere diameter and (F) Number of spheres per 200 cells (G) Western blot analysis of SOX2 and OCT4 on A549 and NCI-H460 cells. \* represented  $p < 0.05$  as compared to untreated cells. Similarly, # represented  $p < 0.05$  as compared to IC<sub>25</sub>, \$ represented  $p < 0.05$  as compared to IC<sub>50</sub>. Data represented as means  $\pm$  SEM from different experiments in triplicate. The results were compared using ANOVA, followed by a Tukey's multiple comparison post-hoc analysis.

region. A moderate expression of p53 and caspase-3 was noted in 50 mg/kg taxifolin (Fig. 12(i)F, (ii)F) and 50 mg/kg ruthenium-p-cymene treated group (Fig. 12(i)G, (ii)G). Carcinogen control group exhibited significant upregulation of Akt (Fig. 12(iii)B), mTOR (Fig. 12(iv)B) and  $\beta$ -catenin (Fig. 12(v)B) expression on the alveolar wall, bronchiolar epithelial region with bronchiolar and vascular cytoplasmic localization in comparison to normal control (Fig. 12(iii)A-(v)A) ( $p < 0.05$ ). The complex (50, 100, 200 mg/kg) treatment significantly ( $p < 0.05$ ) downregulates the Akt (Fig. 12(iii)C-E), mTOR (Fig. 12(iv)C-E) and  $\beta$ -catenin (Fig. 12(v)C-E) expression. A significant expression of Akt, mTOR and  $\beta$ -catenin was also observed for 50 mg/kg taxifolin (Fig. 12(iii)F-(v)F) and 50 mg/kg ruthenium-p-cymene treated group (Fig. 12(iii)G-(v)G).

### 3.5.3. Taxifolin ruthenium-p-cymene complex downregulates Ki-67 level

The cells with Ki-67 labeling showcased a discrete nuclear localization and brown stain which were used for the cellular quantification. The %Ki-67 labeled cells was measured by the labeling index (LI) (Table 8). The carcinogen control group (Fig. 13(i)B) showed highest expression of Ki-67 as compared to the normal control group ( $p < 0.05$ ) (Fig. 13(i)A). The expression of Ki-67 was significantly downregulated in complex treated group (Fig. 13(i)C-E). Moreover, a significantly

high cellular proliferation was also noted in the 50 mg/kg taxifolin (Fig. 13(i)F) and 50 mg/kg ruthenium-p-cymene (Fig. 13(i)G) treated group ( $p < 0.05$ ).

### 3.5.4. Taxifolin ruthenium-p-cymene complex induces apoptosis

The apoptosis assay was conducted to evaluate the incidences of apoptosis in the lung cancer. The apoptotic cells were identified by their brown staining due to chromogen treatment (Fig. 13(ii)). The normal control group (Fig. 13(ii)A) denoted a moderate expression of TUNEL-positive cells. Whereas, significantly ( $p < 0.05$ ) low number of apoptotic cells were noted in the carcinogen control (Fig. 13(ii)B) in comparison to normal control. A significantly ( $p < 0.05$ ) high number of apoptotic cells were noted in the complex treated group (Fig. 13(ii)C-E) as compared to carcinogen control. The 50 mg/kg taxifolin (Fig. 13(ii)F) and 50 mg/kg ruthenium-p-cymene (Fig. 13(ii)G) treated group showed very few apoptotic cells. An average of 4–5 apoptotic cells in the field of 700 cells were identified in carcinogen control. On the other hand, 11–12 TUNEL-positive cells were quantified in 200 mg/kg complex treated group (Table 8).

The R value is expressed as the ratio of cell proliferation to apoptosis. In the carcinogen control group, the increased R value designated the enhanced proliferative activity of the cancer cells but treatment the complex significantly decreased R

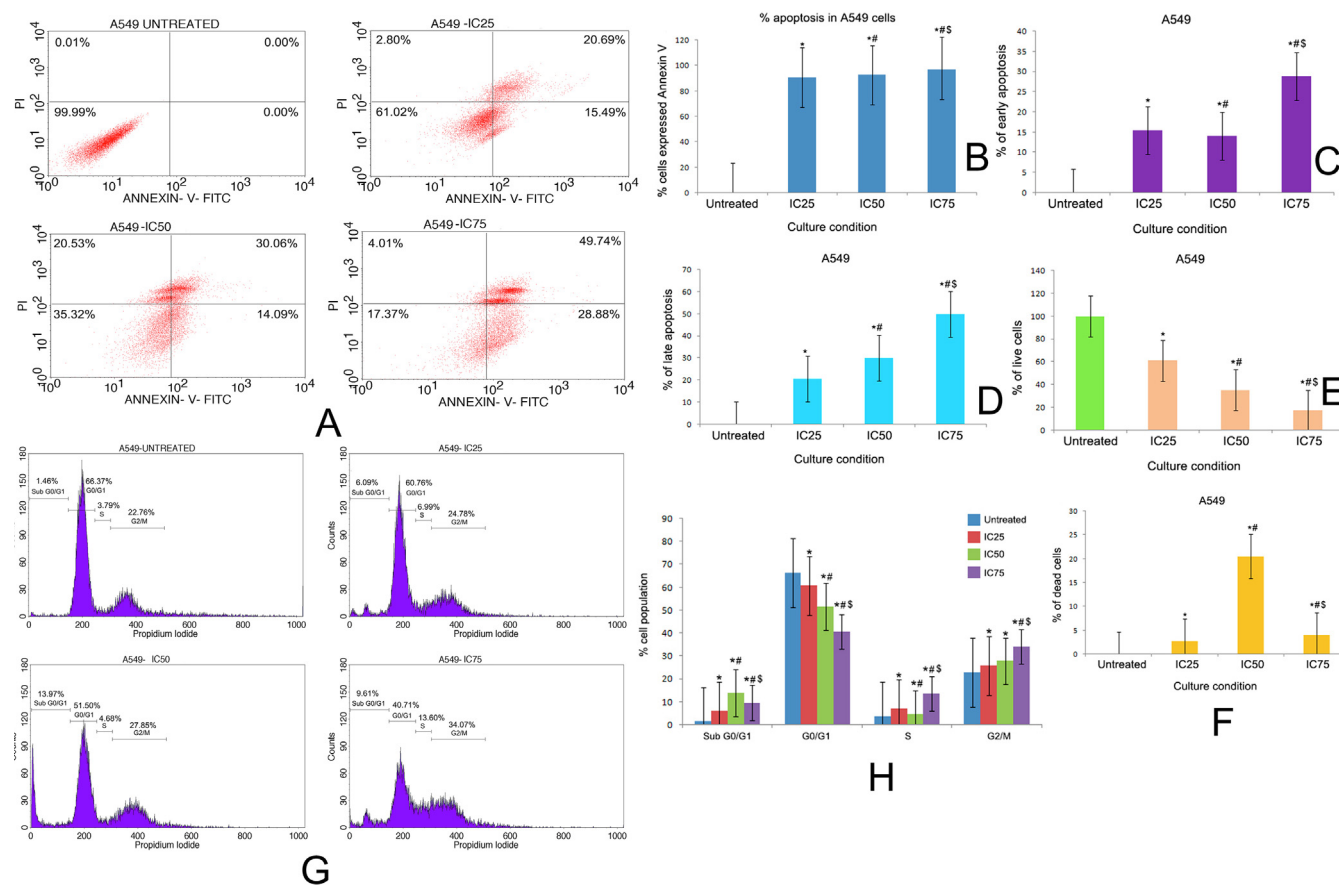


**Fig. 8** (A) Quadrangular plots representing the Annexin V/PI expression in A549 cells upon culturing in the presence and absence of taxifolin ruthenium-p-cymene complex with IC<sub>25</sub>, IC<sub>50</sub> and IC<sub>75</sub> concentrations. Percentage of (B) apoptosis, (C) early apoptosis, (D) late apoptosis, (E) live cells, and (F) dead cells in A549 cells at different culture conditions. (G) Distribution of cell cycle phases in A549 cells upon culturing in the presence and absence of taxifolin ruthenium-p-cymene complex with IC<sub>25</sub>, IC<sub>50</sub> and IC<sub>75</sub> concentrations (H) Quantitative analysis of cell cycle phase distribution in A549 cells. \* represented  $p < 0.05$  as compared to untreated cells. Similarly, # represented  $p < 0.05$  as compared to IC<sub>25</sub>, \$ represented  $p < 0.05$  as compared to IC<sub>50</sub>. Data represented as means  $\pm$  SEM from different experiments in triplicate. The results were compared using ANOVA, followed by a Tukey's multiple comparison post-hoc analysis.

value due to induction of apoptosis and inhibition of cell proliferation.

#### 4. Discussion

In the recent years, lung cancer has been identified as the most prevalent cancer which in turn mandates the discovery of novel therapeutic strategies to combat cancer related mortality. In this instance, the heterogenic nature of lung cancer stem cells abrogates the inhibitory effect of the traditional chemotherapeutic agents (Lin, 2019). Thus, in the upcoming years the strategic designing of multi-targeted anticancer compounds is the crucial aspect of cancer therapy to overcome the cancer stem cell mediated survival approach of cancer cells.

The present research work was focused on synthesizing novel flavonoid based organometallic complex and the evaluation of its chemotherapeutic activity in lung cancer. A number of proteins are involved in the initiation and propagation of lung cancer. The molecular docking study was carried out to identify the specific target proteins for the novel organometallic complex through which the complex supposed to alter the lung cancer incidences in lung cancer cell line as well as in lung

cancer bearing animal model system. According to the molecular docking study the complex exhibits a potent binding affinity for the target proteins such as PI3K, EGFR, and  $\beta$ -catenin that promote the effective binding of the complex to the target proteins. Additionally, it would also endorse respective downstream signaling cascade by acting as an agonist or antagonist to inhibit the lung cancer.

In connection with this, the ruthenium-p-cymene based organometallic complex was synthesized and characterized by various spectroscopical techniques to confirm the formation of taxifolin ruthenium-p-cymene complex. The UV-visible spectroscopical analysis showed the maximum shifting at the band I position of taxifolin due to the formation of the metal complex through  $n - \pi^*$  transition. This confirms the metal complex formation through the cinnamoyl moiety of taxifolin. The interaction between taxifolin and ruthenium-p-cymene dimer molecule was investigated by Job's method and it was found that 1 mol of taxifolin reacts with 2 mol of ruthenium-p-cymene (dimer of ruthenium-p-cymene) and gives maximum yield for the desired complex. The IR spectroscopy of the complex showed the appearance of the peak for ruthenium-oxide bond at  $628.6 \text{ cm}^{-1}$  which was absent in

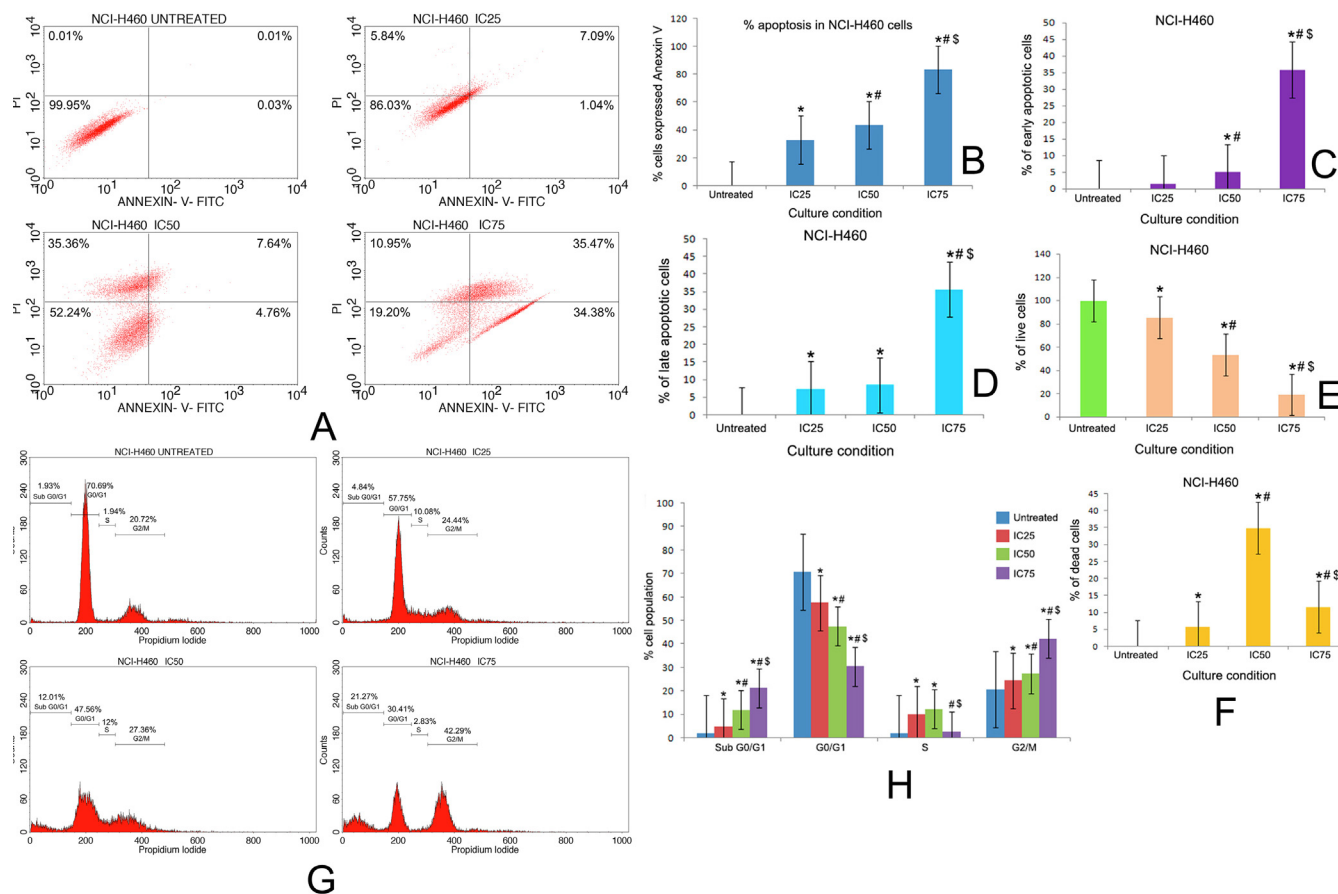


**Fig. 9** (A) Quadrangular plots representing the Annexin V/PI expression in NCI-H460 cells upon culturing in the presence and absence of taxifolin ruthenium-p-cymene complex with IC<sub>25</sub>, IC<sub>50</sub> and IC<sub>75</sub> concentrations. Percentage of (B) apoptosis, (C) early apoptosis, (D) late apoptosis, (E) live cells, and (F) dead cells in NCI-H460 cells at different culture conditions. (G) Distribution of cell cycle phases in NCI-H460 cells upon culturing in the presence and absence of taxifolin ruthenium-p-cymene complex with IC<sub>25</sub>, IC<sub>50</sub> and IC<sub>75</sub> concentrations (H) Quantitative analysis of cell cycle phase distribution in NCI-H460 cells. \* represented  $p < 0.05$  as compared to untreated cells. Similarly, # represented  $p < 0.05$  as compared to IC<sub>25</sub>, \$ represented  $p < 0.05$  as compared to IC<sub>50</sub>. Data represented as means  $\pm$  SEM from different experiments in triplicate. The results were compared using ANOVA, followed by a Tukey's multiple comparison post-hoc analysis.

the FTIR spectrum of taxifolin which suggested the formation of (Ru-O) bond through O-carbonyl group at 4 position and 3-OH group of taxifolin. The mass spectroscopy analysis illustrated the molecular ion peak of the complex at  $m/z$  573.01 which was confirmed from the theoretical monoisotopic mass value of the complex that is 573.98. The <sup>1</sup>H NMR spectroscopy depicted the absence of 3-OH group proton peak which further confirms that complexation has occurred through the 3-OH hydroxyl group of taxifolin. The appearance of sharp peaks in the X-ray Diffractogram strongly suggested the crystalline nature of the complex. Moreover, it also demonstrated the polycrystalline phase of taxifolin ruthenium-p-cymene complex. The scanning electron microscopic pictures at 50X, 4000X, 6000X and 10000X confirms the orthorhombic crystal structure of the complex with sharp edges and symmetrical structures.

Antioxidant property of various flavonoids is considerably linked to their molecular structure. In our present study the taxifolin ruthenium-p-cymene complex showed slightly less antioxidant potential than the free taxifolin in DPPH but displayed more antioxidant potential for FRAP and ABTS radi-

cal scavenging activity. This increased antioxidant activity of the complex can be attributed to the presence of hydroxyl groups and their hydrogen atom donating capability which is facilitated through the chelation of ruthenium metal to the taxifolin moiety. Moreover, the complexation enhances the proton donating ability of the complex which leads to the end of the chain reaction and increases the electron transfer from taxifolin which corresponds to the redox potential of the complex.

The chemotherapeutic activity of taxifolin ruthenium-p-cymene complex was investigated in A549 and NCI-H460 lung cancer cell line from the perspective of stemness and EMT regulation. The cell viability assay demonstrated that, the complex inhibited the viability of A549 and NCI-H460 cells dose dependently. The IC<sub>50</sub> value calculated from cell viability assay was found to be 187.19  $\mu$ M and 108.62  $\mu$ M for A549 and NCI-H460 cell lines respectively. Subsequently, the chemotherapeutic doses (IC<sub>25</sub>, IC<sub>50</sub> and IC<sub>75</sub>) of the complex were determined. The induction of cellular death was visualized by the DAPI analysis which demonstrated maximum nuclear condensation at IC<sub>75</sub> of the complex in A549 and NCI-H460 cell line respec-

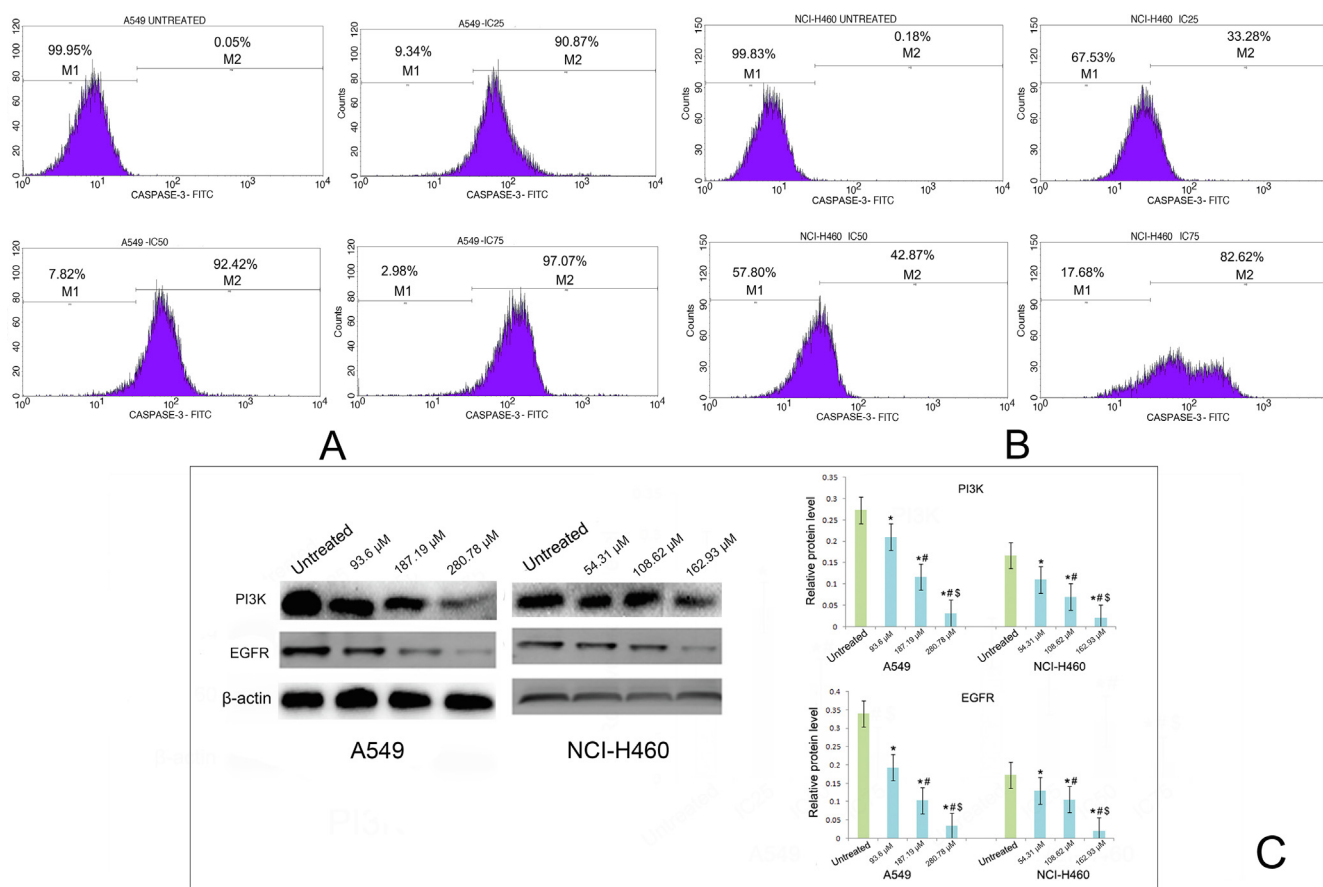


**Fig. 10** Effect of taxifolin ruthenium-p-cymene complex on the expression of caspase-3 in (A) A549 cells and (B) NCI-H460 cells. (C) Western blot analysis of PI3K and EGFR on A549 and NCI-H460 cells. \* represented  $p < 0.05$  as compared to untreated cells. Similarly, # represented  $p < 0.05$  as compared to IC<sub>25</sub>, \$ represented  $p < 0.05$  as compared to IC<sub>50</sub>. Data represented as means  $\pm$  SEM from different experiments in triplicate. The results were compared using ANOVA, followed by a Tukey's multiple comparison post-hoc analysis.

tively. Additionally, the colony formation ability of the cancer cells was significantly inhibited due to the treatment with taxifolin ruthenium-p-cymene complex.

Stemness plays the pivotal role in the initiation, metastasis, and therapy resistance of NSCLC through the regulation of several intracellular pathways which include Wnt/ $\beta$ -catenin, PI3K/Akt/mTOR pathway (Lin, 2019). In this research, the treatment with taxifolin ruthenium-p-cymene complex dose dependently downregulated the incidence of stemness in both cell lines. The complex treated cells significantly inhibited the sphere formation and downregulated the expression of stem cell markers such as SOX2 and OCT4 in both the cell line. In addition, the results further portray the complex mediated inhibition of PI3K/Akt signaling that might be responsible for the inhibition of stemness in the cancer cells.

It has been observed that, the EMT is the most primary event which takes place before the onset of cancer metastasis (Yeung and Yang, 2017). Recent studies reported that, the cancer stem cells are responsible for the cancer metastasis through the modulation of Wnt/ $\beta$ -catenin, PI3K/Akt/mTOR pathway (Lin, 2019). Therefore, the inhibition of stemness due to taxifolin ruthenium-p-cymene therapy could reduce the metastasis via preventing EMT in lung cancer cell lines. Moreover, the EMT has also been found to be regulated by

various growth factors such as EGFR. In this study, the inhibition of EMT in the cancer cell was investigated through the transwell migration assay. The result demonstrated that, taxifolin ruthenium-p-cymene treatment dose dependently inhibited the invasive cells in both A549 and NCI-H460 cell lines. Furthermore, the downregulation of N-cadherin and upregulation of E-cadherin expression was noted which suggested the inhibition of EMT in both the cell lines. The expression of EGFR was also found to be downregulated which signified reduction of EMT mediated metastasis through the inhibition of EMT regulating signaling cascade and stemness of the cancer cells.

In addition, the flow cytometric analysis demonstrated the induction of apoptosis in A549 and NCI-H460 cell line upon the treatment with the novel complex. A large number of cells at apoptotic stage were identified in the complex treated group, where the treatment with IC<sub>75</sub> showed maximum apoptosis in A549 (97.07%) and NCI-H460 (82.62%) cells. Moreover, a significant percentage of early apoptosis, late apoptosis and dead cells were noted in the complex treated group in both the cell line. Whereas, a dose dependent decrease in the percentage of live cells was observed in the complex treated cells.

The loss of cell cycle regulation followed by uncontrolled cellular growth is one of the important aspects of cancer cells



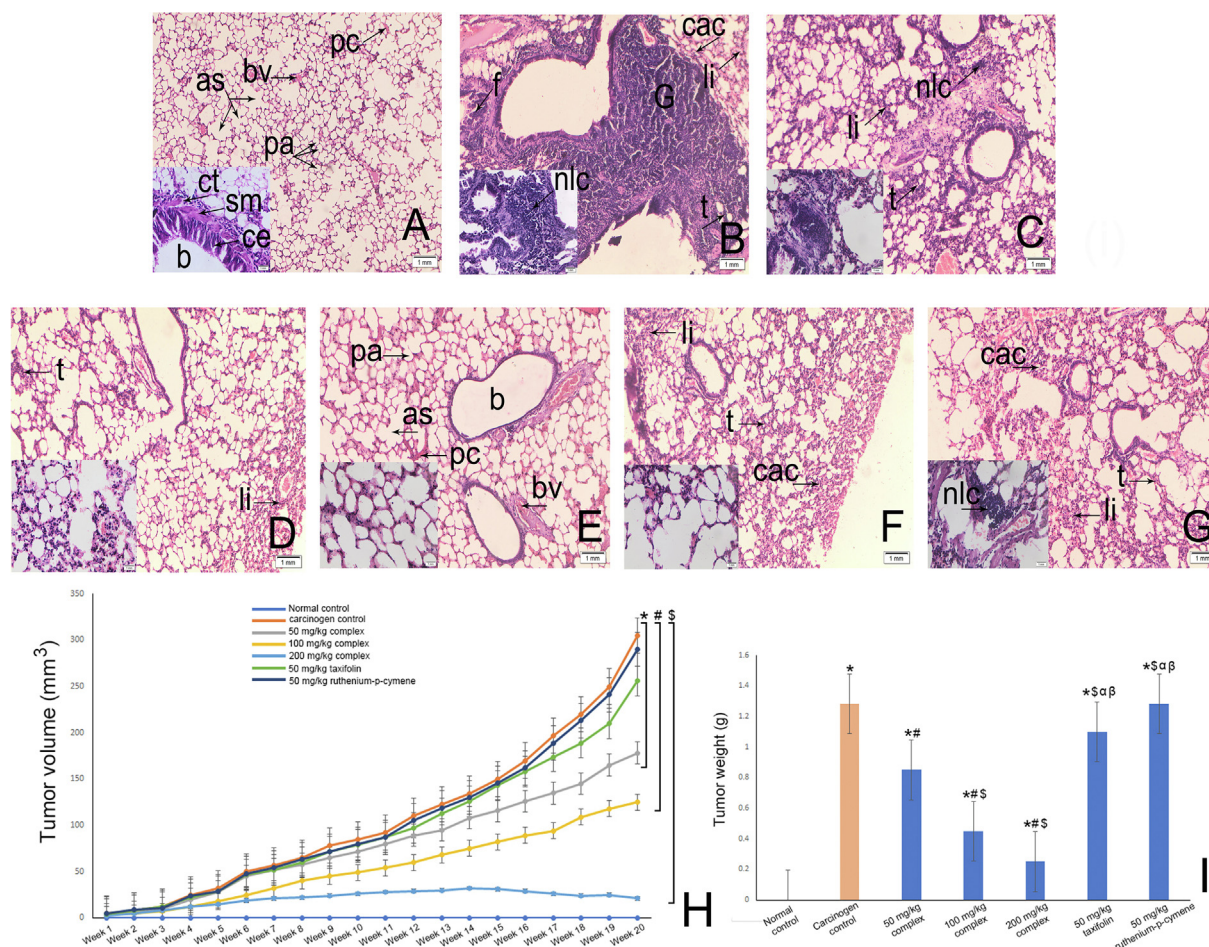


**Fig. 11** Histopathological appearance of lung at 10X [inset 40X]. (A) Normal control group showed bronchiole (*b*), pulmonary alveoli (*pa*), alveolar sac (*as*), blood vessels (*bv*), pulmonary capillary (*pc*), columnar epithelium (*ce*), smooth muscle (*sm*). (B) Carcinogen control group depicted thickened alveolar walls (*t*), congested alveolar cavity (*cac*), nodular lymphocytic collection (*nlc*), lymphocyte infiltration (*li*) in alveolar space, severe fibrosis (*f*) and formation of granuloma (*g*). (C) 50 mg/kg taxifolin ruthenium-p-cymene complex treated group showed thickened alveolar walls (*t*), nodular lymphocytic collection (*nlc*) and lymphocyte infiltration (*li*) in alveolar space. (D) 100 mg/kg taxifolin ruthenium-p-cymene complex treated group showed thickened alveolar walls (*t*) and lymphocyte infiltration (*li*) in alveolar space. (E) 200 mg/kg taxifolin ruthenium-p-cymene complex treated group restored normal morphological architecture of carcinogen induced lung tissue. (F) 50 mg/kg taxifolin treated group depicted thickened alveolar walls (*t*), congested alveolar cavity (*cac*) and lymphocyte infiltration (*li*) in alveolar space. (G) 50 mg/kg ruthenium-p-cymene treated group depicted thickened alveolar walls (*t*), congested alveolar cavity (*cac*), nodular lymphocytic collection (*nlc*) and lymphocyte infiltration (*li*) in alveolar space. Effect of taxifolin ruthenium-p-cymene complex on the (H) tumor volume (mm<sup>3</sup>) and (I) tumor weight (g).

(Jin and El-Deiry, 2005). Thus, the cell cycle regulation via induction of cell cycle arrest is a major chemotherapeutic strategy which allows the accumulation of DNA damage and promotes apoptosis in cancer cells. The activation of apoptotic events in the cancer cells was also determined via the investigation of caspase-3 expression. The flow cytometric analysis demonstrated an increased level of caspase-3 labelled cells in the complex treated group which signified the caspase-3 mediated apoptosis induction in the cancer cells. The effect of the complex on cell cycle phase distribution was also investigated in A549 and NCI-H460 cells through flow cytometry. The result from the cell cycle analysis designated that, the treatment with the complex caused cellular arrest in sub G0/G1 phase (apoptotic phase), S phase (synthetic phase) and G2/M phase of cell cycle and ultimately stimulated the apoptotic events in lung cancer cells.

The *in vivo* chemotherapeutic study was carried out on B( $\alpha$ )P induced lung cancer model of Balb/c mice. The histopathology of lung showed severe pulmonary fibrosis and granuloma formation in the carcinogen control group. In addition, congestion in alveolar cavity and severe lymphocytic infiltration in the alveolar space was identified in the carcinogen control. However, taxifolin ruthenium-p-cymene complex treatment significantly decreased the pulmonary fibrosis and restored normal cellular architecture of lung tissue. Along with that, the tumor burden was also significantly lowered in the complex treated group. These findings suggested the anticancer efficacy of the complex against B( $\alpha$ )P induced lung carcinoma.

The expression profile of p53, caspase-3, Akt, mTOR, and  $\beta$ -catenin was determined in the lung tissue by immunohistochemical analysis. Several studies have demonstrated that, the mutation in the tumor suppressor protein p53 is directly

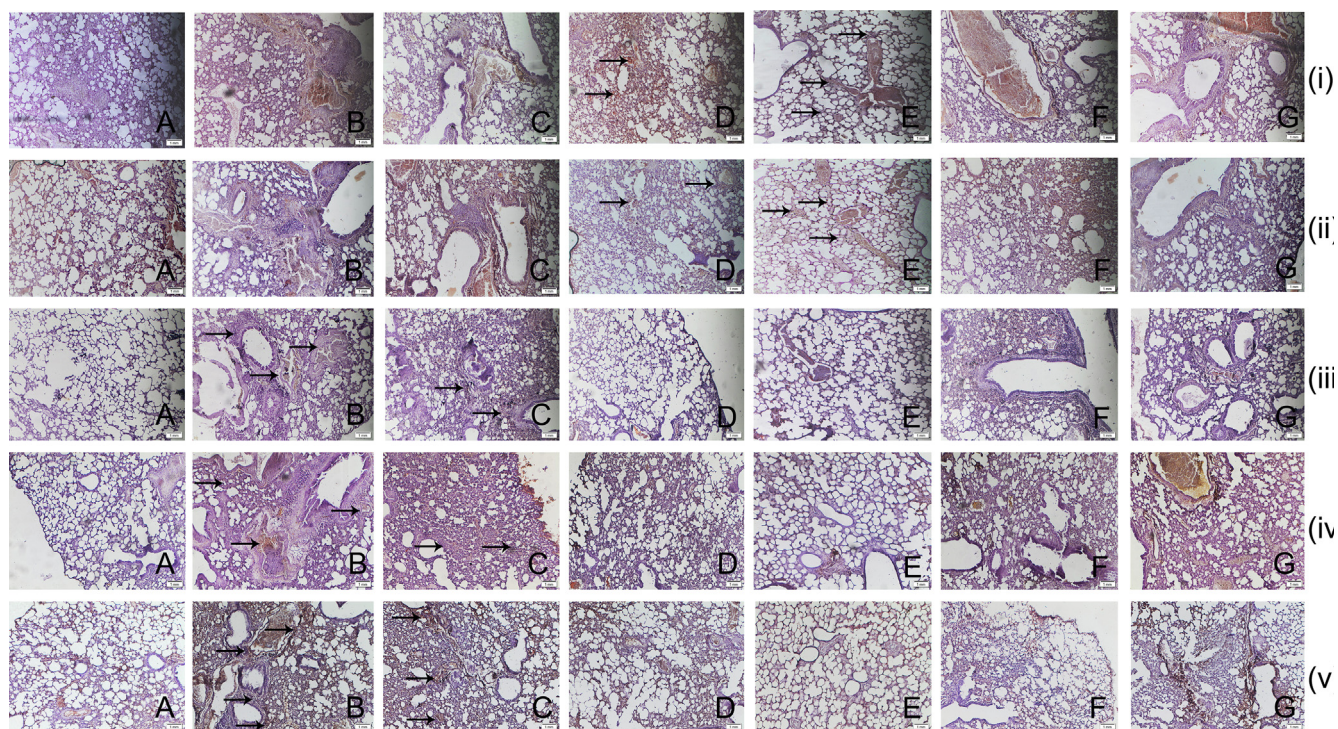


**Fig. 12.** The immunohistochemical analysis of [i] p53 [ii] caspase-3, [iii] Akt, [iv] mTOR, and [v]  $\beta$ -catenin expression in the lung tissues at 10X magnification of (A) normal control, (B) carcinogen control, (C) 50 mg/kg complex, (D) 100 mg/kg complex, (E) 200 mg/kg complex, (F) 50 mg/kg taxifolin, and (G) 50 mg/kg ruthenium-p-cymene treated group, represented by black arrows.

**Table 7** The effect of taxifolin, ruthenium-p-cymene and taxifolin ruthenium-p-cymene complex on the expression of p53, caspase-3, Akt, mTOR and  $\beta$ -catenin.

Groups	p53 <sup>§</sup>	Caspase-3 <sup>§</sup>	Akt <sup>§</sup>	mTOR <sup>§</sup>	$\beta$ -catenin <sup>§</sup>
Normal control	8.25 $\pm$ 0.1	5 $\pm$ 0.5	8.83 $\pm$ 0.1	7.35 $\pm$ 0.2	4.68 $\pm$ 0.1
Carcinogen control	3.82 $\pm$ 0.6*	2.17 $\pm$ 0.1*	22.22 $\pm$ 0.1*	25.97 $\pm$ 0.1*	22.98 $\pm$ 0.1*
50 mg/kg complex	4.07 $\pm$ 0.1*	9.85 $\pm$ 0.1*#	14.98 $\pm$ 0.1*#	14 $\pm$ 0.1*#	18.85 $\pm$ 0.1*#
100 mg/kg complex	6.1 $\pm$ 0.1*# <sup>S</sup>	9.95 $\pm$ 0.1*#	12.87 $\pm$ 0.1*# <sup>S</sup>	12.2 $\pm$ 0.1*# <sup>S</sup>	12 $\pm$ 0.1*# <sup>S</sup>
200 mg/kg complex	7.87 $\pm$ 0.1*# <sup>S<math>\alpha</math></sup>	13.75 $\pm$ 0.1*# <sup>S<math>\alpha</math></sup>	8.23 $\pm$ 0.2*# <sup>S<math>\alpha</math></sup>	8.03 $\pm$ 0.1*# <sup>S<math>\alpha</math></sup>	8.87 $\pm$ 0.1*# <sup>S<math>\alpha</math></sup>
50 mg/kg taxifolin	3.92 $\pm$ 0.1* <sup><math>\alpha\beta</math></sup>	4.17 $\pm$ 0.1*# <sup>S<math>\alpha\beta</math></sup>	17 $\pm$ 0.1*# <sup>S<math>\alpha\beta</math></sup>	20.1 $\pm$ 0.1*# <sup>S<math>\alpha\beta</math></sup>	20.01 $\pm$ 0.1*# <sup>S<math>\alpha\beta</math></sup>
50 mg/kg ruthenium-p-cymene	3.18 $\pm$ 0.1* <sup><math>\alpha\beta</math></sup>	2.98 $\pm$ 0.1*# <sup>S<math>\alpha\beta\gamma</math></sup>	19.13 $\pm$ 0.1*# <sup>S<math>\alpha\beta\gamma</math></sup>	23.15 $\pm$ 0.1*# <sup>S<math>\alpha\beta\gamma</math></sup>	21.05 $\pm$ 0.1*# <sup>S<math>\alpha\beta\gamma</math></sup>

<sup>§</sup> Each score represents the results of 6 slides per rat and 6 rats per group, mean  $\pm$  S.E. (n = 6). Each field was selected randomly for evaluation of percentage of immune-positive cells.

\* significant difference as compared to normal control (p < 0.05).

# significant difference as compared to carcinogen control group (p < 0.05).

<sup>S</sup> significant difference as compared to 50 mg/kg complex treated group (p < 0.05).

<sup>$\alpha$</sup>  significant difference as compared to 100 mg/kg complex treated group (p < 0.05).

<sup>$\beta$</sup>  significant difference as compared to 200 mg/kg complex treated group (p < 0.05).

<sup>$\gamma$</sup>  significant difference as compared to 50 mg/kg taxifolin treated group (p < 0.05).

related to the growth of malignant lesions through the inhibition of tumor suppressive pathway (Rivlin et al., 2011). An increased expression of p53 is responsible for the caspase-3 mediated intrinsic apoptosis in the cancer cells (Zhuo et al., 2015). The suppression of apoptosis can directly facilitate the neoplastic transformation by promoting tumour growth, metastasis, survival, and therapeutic resistance. Recent studies reported that, the PI3K/Akt/mTOR pathway is widely activated in NSCLC (Papadimitrakopoulou, 2012) due to the

alteration of various upstream regulators such as EGFR which results in constitutive activation of the intracellular signaling cascade. In this instance, the phosphorylated Akt has been found to be mostly altered in several lung cancer incidences (Tsurutani et al., 2006). Furthermore, the upregulation of PI3K/Akt/mTOR pathway is also associated with the development of drug resistance against EGFR targeted therapy (Gadgeel and Wozniak, 2013). The development of EGFR mutated lung carcinoma is also responsible for the aberrant

**Table 8** Cell proliferation and apoptosis in lung tissue.

Groups	Ki-67-LI <sup>§</sup>	AI (%) <sup>§</sup>	R = Ki-67-LI/AI
Normal control	15.5 ± 0.1	0.11 ± 0.01	148 ± 11.23
Carcinogen control	36.88 ± 0.1*	0.03 ± 0.01*	1689 ± 445.59*
50 mg/kg complex	23.88 ± 0.1* <sup>#</sup>	0.06 ± 0.005*	439 ± 41.75 <sup>#</sup>
100 mg/kg complex	15 ± 0.4 <sup>#S</sup>	0.09 ± 0.01 <sup>#S</sup>	170 ± 10.95 <sup>#</sup>
200 mg/kg complex	6.96 ± 0.1* <sup>#Sα</sup>	0.12 ± 0.004 <sup>#Sα</sup>	56 ± 1.36 <sup>#</sup>
50 mg/kg taxifolin	29.06 ± 0.1* <sup>#Sαβ</sup>	0.04 ± 0.01* <sup>αβ</sup>	1142 ± 375.34* <sup>αβ</sup>
50 mg/kg ruthenium-p-cymene	33 ± 0.1* <sup>#Sαβγ</sup>	0.03 ± 0.01* <sup>αβ</sup>	1481 ± 405.58* <sup>αβ</sup>

LI = Labelling index, Ki-67-LI = percentage of Ki-67 labelled cells/total number of cells counted, AI = Apoptotic index. R = Ki-67-LI/AI. AI was calculated as the percentage of TUNEL positive cells/total number of cells counted. Values represent mean ± S.E. (n = 6).

<sup>S</sup> significant difference as compared to 50 mg/kg complex treated group (p < 0.05).

<sup>α</sup> significant difference as compared to 100 mg/kg complex treated group (p < 0.05).

<sup>β</sup> significant difference as compared to 200 mg/kg complex treated group (p < 0.05).

<sup>§</sup> Total number of six slides was evaluated per rat and 6 rats per group. Each field consisted of 700 cells.

\* significant difference as compared to normal control (p < 0.05).

<sup>#</sup> significant difference as compared to carcinogen control group (p < 0.05).

<sup>γ</sup> significant difference as compared to 50 mg/kg taxifolin treated group (p < 0.05).

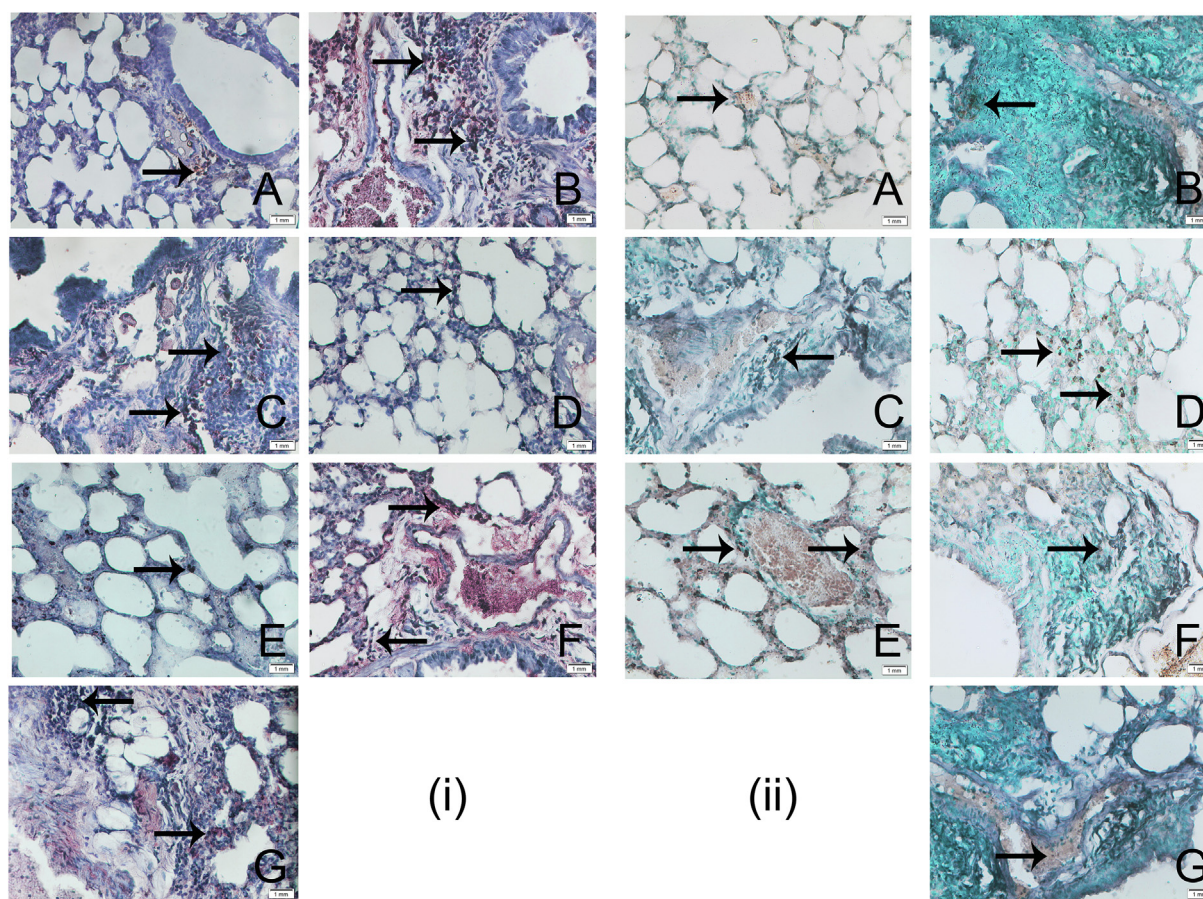


**Fig. 13** The immunohistochemical analysis of **[i]** Ki-67 expression and **[ii]** TUNEL-positive apoptotic cells in the lung tissue at 40X magnification of (A) normal control, (B) carcinogen control, (C) 50 mg/kg complex, (D) 100 mg/kg complex, (E) 200 mg/kg complex, (F) 50 mg/kg taxifolin, and (G) 50 mg/kg ruthenium-p-cymene treated group, represented by black arrows. Approximately 700 cells were counted per field, 10 fields were examined per slide.

activation of  $\beta$ -catenin (Nakayama et al., 2014). Recent studies further demonstrated that, the activation of Wnt/ $\beta$ -catenin pathway caused severe metastasis of lung cancer (Nguyen

et al., 2009). Thus, pharmacological inhibition of  $\beta$ -catenin is directly associated with the suppression of lung cancer initiation, metastasis, and drug resistance (Nakayama et al.,

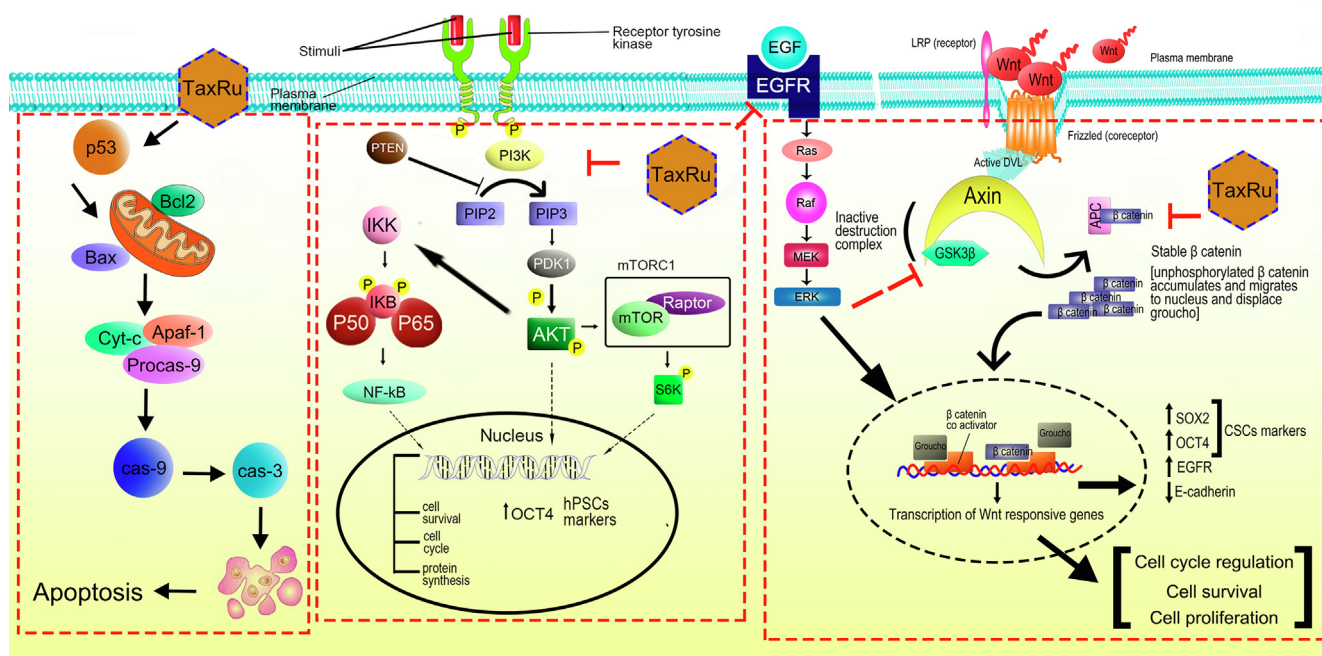


**Fig. 14** The possible mechanism of action of taxifolin ruthenium-p-cymene complex against lung carcinoma.

2014). The immunohistochemical analysis of lung tissue exhibited decreased expression of p53 and caspase-3 in the carcinogen control group with an increased expression of Akt, mTOR, and  $\beta$ -catenin. The treatment with taxifolin ruthenium-p-cymene complex showed significant upregulation of p53 and caspase-3 expression with downregulation of Akt, mTOR, and  $\beta$ -catenin expression in lung which suggest the inhibition of lung cancer through the induction of p53/caspase-3 mediated apoptosis and suppression of Akt/mTOR/ $\beta$ -catenin pathway regulated cell survival strategies.

The Ki-67 has been identified as a potent prognostic marker for the lung cancer which involved in the regulation of cellular proliferation (Martin et al., 2004). In this regard, an increased Ki-67 expression and low apoptotic index were considered as progressive cancer (Baisch, 2002). The cell proliferation assay exhibited an upregulation of Ki-67 expression with increased labelling index in the carcinogen control group. Whereas, the TUNEL assay demonstrated a significantly low number of TUNEL positive apoptotic cells with low apoptotic index in the carcinogen control group. On the other hand, the complex treated group significantly downregulated the expression of Ki-67 and reduced the labelling index with increased level of apoptotic cells in the lung tissue. Thus, the treatments with the complex reduced the cancer cell propagation and promoted apoptosis in the cancer cells. Consistent with this in vivo report, the in vitro study also depicted the induction of cellular death through p53/caspase-3 mediated apoptosis and inhibition of cell proliferation via downregulating the PI3K/EGFR pathway in the A549 and NCI-H460 cancer cells.

## 5. Conclusion

Taking together, it was concluded that, the taxifolin ruthenium-p-cymene complex displayed significant anticancer efficacy against both A549 and NCI-H460 cell line and B( $\alpha$ )P induced lung cancer

model of mice through the induction of p53/caspase-3 mediated intrinsic apoptotic events and cell cycle arrest in sub G0/G1 phase, S phase and G2/M phase. Additionally, the taxifolin ruthenium-p-cymene complex inhibited cancer cell viability, stemness, and EMT in both in vitro and in vivo model systems through the alteration of upstream regulatory pathways such as PI3K/Akt/mTOR/EGFR pathway and expression of stem cell markers including SOX2 and OCT4 that eventually abrogated the EMT mediated metastasis of cancer cells. After careful consideration of in vivo and in vitro experimentation the possible multi-targeted molecular mechanistic pathway of the complex against lung cancer stemness has been illustrated in Fig. 14. These outcomes strongly indicated the prospective effect of taxifolin ruthenium-p-cymene complex against lung cancer and firmly supported the potential use of this novel chemotherapeutic agent in clinical settings.

## Declaration of Competing Interest

The authors declare that they have no known competing financial interests or personal relationships that could have appeared to influence the work reported in this paper.

## Acknowledgements

The authors are grateful to the Department of Pharmacy, NSHM Knowledge Campus- Kolkata for their continuous support and encouragement throughout the study.

## Authorship contribution statement

All authors contributed to the study conception and design. Material preparation, data collection, and draft of the manuscript were written by Abhijit Das, Ishita Seal and Sidhanta Sil. The data analysis and supervision were done by Balaram Ghosh and Sandipan Dasgupta. Final review and editing were

done by Souvik Roy. All authors read and approved the final manuscript.

### Funding

This research did not receive any specific grant from funding agencies in the public, commercial, or not-for-profit sectors.

### Appendix A. Supplementary material

Supplementary data to this article can be found online at <https://doi.org/10.1016/j.arabjc.2023.104995>.

### References

- Allardyce, C.S., Dyson, P.J., 2001. Ruthenium in medicine: current clinical uses and future prospects. *Platinum Metals Rev.* 45, 62–69.
- Baisch, H., 2002. Elevated Ki-67 expression is correlated with TNF $\alpha$ - and IFN $\gamma$ -induced apoptosis in tumour cells. *Cell Prolif.* 35, 333–342. <https://doi.org/10.1046/j.1365-2184.2002.00243.x>.
- Benzie, I.F., Strain, J.J., 1996. The ferric reducing ability of plasma (FRAP) as a measure of “antioxidant power”: the FRAP assay. *Anal. Biochem.* 239, 70–76. <https://doi.org/10.1006/abio.1996.0292>.
- Bugaric, T., Habtemariam, A., Deeth, R.J., Fabbiani, F.P., Parsons, S., Sadler, P.J., 2009. Ruthenium(II) arene anticancer complexes with redox-active diamine ligands. *Inorg. Chem.* 48, 9444–9453. <https://doi.org/10.1021/ic9013366>.
- Butler, M.S., 2006. The role of natural product chemistry in drug discovery. *J. Nat. Prod.* 69, 172. <https://doi.org/10.1021/np040106y>.
- Clevers, H., 2006. Wnt/beta-catenin signaling in development and disease. *Cell* 127, 469–480. <https://doi.org/10.1016/j.cell.2006.10.018>.
- Córdoba, A., Satué, M., Gómez-Florit, M., Hierro-Oliva, M., Petzold, C., Lyngstadaas, S.P., González-Martín, M.L., Monjo, M., Ramis, J.M., 2015. Flavonoid-modified surfaces: multifunctional bioactive biomaterials with osteopromotive, anti-inflammatory, and anti-fibrotic potential. *Adv. Healthc. Mater.* 4, 540–549. <https://doi.org/10.1002/adhm.201400587>.
- Dethlefsen, L.A., Prewitt, J.M., Mendelsohn, M.L., 1968. Analysis of tumor growth curves. *J. Natl. Cancer Inst.* 40, 389–405. <https://doi.org/10.1093/jnci/40.2.389>.
- Dyson, P.J., 2017. Systematic design of a targeted organometallic antitumour drug in pre-clinical development. *Chimia* 61, 698–1670.
- Gadgeel, S.M., Wozniak, A., 2013. Preclinical rationale for PI3K/Akt/mTOR pathway inhibitors as therapy for epidermal growth factor receptor inhibitor-resistant non-small-cell lung cancer. *Clin. Lung Cancer* 14, 322–332. <https://doi.org/10.1016/j.clcc.2012.12.001>.
- Griffin, S.P., Bhagooli, R., 2004. Measuring antioxidant potential in corals using the FRAP assay. *J. Exp. Mar. Biol. Ecol.* 302, 201–211. <https://doi.org/10.1016/j.jembe.2003.10.008>.
- Hassan, M., Watari, H., Abu Almaaty, A., Ohba, Y., Sakuragi, N., 2014. Apoptosis and molecular targeting therapy in cancer. *Biomed. Res. Int.* 2014. <https://doi.org/10.1155/2014/150845>
- Heim, K.E., Tagliaferro, A.R., Bobilya, D.J., 2002. Flavonoid antioxidants: chemistry, metabolism and structure-activity relationships. *J. Nutr. Biochem.* 13, 572–584. [https://doi.org/10.1016/s0955-2863\(02\)00208-5](https://doi.org/10.1016/s0955-2863(02)00208-5).
- Huang, H., Zhang, P., Yu, B., Chen, Y., Wang, J., Ji, L., Chao, H., 2014. Targeting nucleus DNA with a cyclometalated dipyrrophenazine ruthenium(II) complex. *J. Med. Chem.* 57, 8971–8983. <https://doi.org/10.1021/jm501095r>.
- Iacopetta, D., Grande, F., Caruso, A., Mordocco, R.A., Plutino, M. R., Scrivano, L., Ceramella, J., Muià, N., Saturnino, C., Puoci, F., Rosano, C., Sinicropi, M.S., 2017. New insights for the use of quercetin analogs in cancer treatment. *Future Med. Chem.* 9, 2011–2028. <https://doi.org/10.4155/fmc-2017-0118>.
- Jin, Z., El-Deiry, W.S., 2005. Overview of cell death signaling pathways. *Cancer Biol. Ther.* 4, 139–163. <https://doi.org/10.4161/cbt.4.2.1508>.
- Kumar, S., Pandey, A.K., 2013. Phenolic content, reducing power and membrane protective activities of *Solanum xanthocarpum* root extracts. *VEGETOS: Int. J. Plant Res.* 26, 301–307. <https://doi.org/10.5958/j.2229-4473.26.1.043>.
- Lin, C.C., 2019. Challenges of the phase I drug development in non-small cell lung cancer. *Chin. Clin. Oncol.* 8, 25. <https://doi.org/10.21037/cco.2019.06.03>.
- Mani, S.A., Guo, W., Liao, M.J., Eaton, E.N., Ayyanan, A., Zhou, A. Y., Brooks, M., Reinhard, F., Zhang, C.C., Shipitsin, M., Campbell, L.L., Polyak, K., Brisken, C., Yang, J., Weinberg, R. A., 2008. The epithelial-mesenchymal transition generates cells with properties of stem cells. *Cell* 133, 704–715. <https://doi.org/10.1016/j.cell.2008.03.027>.
- Martin, B., Paesmans, M., Mascaux, C., Berghmans, T., Lothaire, P., Meert, A.P., Lafitte, J.J., Sculier, J.P., 2004. Ki-67 expression and patients survival in lung cancer: systematic review of the literature with meta-analysis. *Br. J. Cancer* 91, 2018–2025. <https://doi.org/10.1038/sj.bjc.6602233>.
- Masciale, V., Grisendi, G., Banchelli, F., D’Amico, R., Maiorana, A., Sighinolfi, P., Pinelli, M., Lovati, E., Stefani, A., Morandi, U., Dominici, M., Aramini, B., 2019. Correlating tumor-infiltrating lymphocytes and lung cancer stem cells: a cross-sectional study. *Ann. Transl. Med.* 7, 619. <https://doi.org/10.21037/atm.2019.11.27>.
- Min, H.Y., Jang, H.J., Park, K.H., Hyun, S.Y., Park, S.J., Kim, J.H., Son, J., Kang, S.S., Lee, H.Y., 2019. The natural compound gracillin exerts potent antitumor activity by targeting mitochondrial complex II. *Cell Death Dis.* 10, 810. <https://doi.org/10.1038/s41419-019-2041-z>.
- Nakayama, S., Sng, N., Carretero, J., Welner, R., Hayashi, Y., Yamamoto, M., Tan, A.J., Yamaguchi, N., Yasuda, H., Li, D., Soejima, K., Soo, R.A., Costa, D.B., Wong, K.K., Kobayashi, S.S., 2014.  $\beta$ -catenin contributes to lung tumor development induced by EGFR mutations. *Cancer Res.* 74, 5891–5902. <https://doi.org/10.1158/0008-5472.CAN-14-0184>.
- Nath, A., Sathishkumar, K., Das, P., Sudarshan, K.L., Mathur, P., 2022. A clinicoepidemiological profile of lung cancers in India - Results from the National Cancer Registry Programme. *Indian J. Med. Res.* 155, 264–272. [https://doi.org/10.4103/ijmr.ijmr\\_1364\\_21](https://doi.org/10.4103/ijmr.ijmr_1364_21).
- Nguyen, D.X., Chiang, A.C., Zhang, X.H., Kim, J.Y., Kris, M.G., Ladanyi, M., Gerald, W.L., Massagué, J., 2009. WNT/TCF signaling through LEF1 and HOXB9 mediates lung adenocarcinoma metastasis. *Cell* 138, 51–62. <https://doi.org/10.1016/j.cell.2009.04.030>.
- Papadimitrakopoulou, V., 2012. Development of PI3K/AKT/mTOR pathway inhibitors and their application in personalized therapy for non-small-cell lung cancer. *J. Thorac. Oncol.* 7, 1315–1326. <https://doi.org/10.1097/JTO.0b013e31825493eb>.
- Pennycooke, J.C., Cox, S., Stushnoff, C., 2005. Relationship of Cold Acclimation, Total Phenolic Content and Antioxidant Capacity with Chilling Tolerance in *Petunia* (Petunia x Hybrid). *Environ. Exp. Bot.* 53, 225–232. <https://doi.org/10.1016/j.envexpbot.2004.04.002>.
- Rahman, M., Islam, M., Biswas, M., Khurshid Alam, A.H.M., 2015. In vitro antioxidant and free radical scavenging activity of different parts of *Tabebuia pallida* growing in Bangladesh. *BMC Res. Notes* 8, 621. <https://doi.org/10.1186/s13104-015-1618-6>.
- Raj Kumar, R., Ramesh, R., Malecki, J.G., 2018. Synthesis and structure of arene ruthenium(II) benzhydrazone complexes: Antiproliferative activity, apoptosis induction and cell cycle anal-

- ysis. *J. Organomet. Chem.* 862, 95–100. <https://doi.org/10.1016/j.jorganchem.2018.03.013>.
- Rivlin, N., Brosh, R., Oren, M., Rotter, V., 2011. Mutations in the p53 tumor suppressor gene: important milestones at the various steps of tumorigenesis. *Genes Cancer* 2, 466–474. <https://doi.org/10.1177/1947601911408889>.
- Sadot, E., Geiger, B., Oren, M., Ben-Ze'ev, A., 2001. Down-regulation of beta-catenin by activated p53. *Mol. Cell Biol.* 21, 6768–6781. <https://doi.org/10.1128/MCB.21.20.6768-6781.2001>.
- Sung, H., Ferlay, J., Siegel, R.L., Laversanne, M., Soerjomataram, I., Jemal, A., Bray, F., 2021. Global Cancer Statistics 2020: GLOBOCAN Estimates of Incidence and Mortality Worldwide for 36 Cancers in 185 Countries. *C.A Cancer J. Clin.* 71, 209–249. <https://doi.org/10.3322/caac.21660>.
- Tsurutani, J., Fukuoka, J., Tsurutani, H., Shih, J.H., Hewitt, S.M., Travis, W.D., Jen, J., Dennis, P.A., 2006. Evaluation of two phosphorylation sites improves the prognostic significance of Akt activation in non-small-cell lung cancer tumors. *J. Clin. Oncol.* 24, 306–314. <https://doi.org/10.1200/JCO.2005.02.4133>.
- Wang, R., Zhu, X., Wang, Q., Li, X., Wang, E., Zhao, Q., Wang, Q., Cao, H., 2020. The anti-tumor effect of taxifolin on lung cancer via suppressing stemness and epithelial-mesenchymal transition *in vitro* and oncogenesis in nude mice. *Ann. Transl. Med.* 8, 590. <https://doi.org/10.21037/atm-20-3329>.
- Yao, R., Cooper, G.M., 1995. Requirement for phosphatidylinositol-3 kinase in the prevention of apoptosis by nerve growth factor. *Science* 267, 2003–2006. <https://doi.org/10.1126/science.7701324>.
- Yeung, K.T., Yang, J., 2017. Epithelial-mesenchymal transition in tumor metastasis. *Mol. Oncol.* 11, 28–39. <https://doi.org/10.1002/1878-0261.12017>.
- Zhang, Y., Wang, X., 2020. Targeting the Wnt/ $\beta$ -catenin signaling pathway in cancer. *J. Hematol. Oncol.* 13, 165. <https://doi.org/10.1186/s13045-020-00990-3>.
- Zhuo, Z., Hu, J., Yang, X., Chen, M., Lei, X., Deng, L., Yao, N., Peng, Q., Chen, Z., Ye, W., Zhang, D., 2015. Ailanthone Inhibits Huh7 Cancer Cell Growth via Cell Cycle Arrest and Apoptosis *In Vitro* and *In Vivo*. *Sci. Rep.* 5, 16185. <https://doi.org/10.1038/srep16185>.